

Pseudoscalar top-Higgs coupling: Exploration of CP-odd observables to resolve the sign ambiguity

Nicolas Mileo,^{1,*} Ken Kiers,^{2,†} Alejandro Szynkman,^{1,‡} Daniel Crane,^{2,§} and Ethan Gegner^{2,¶}

¹*IFLP, CONICET – Dpto. de Física, Universidad Nacional de La Plata, C.C. 67, 1900 La Plata, Argentina*

²*Physics and Engineering Department, Taylor University, 236 West Reade Ave., Upland, IN 46989, USA*

(Dated: March 7, 2016)

Abstract

We present a collection of CP-odd observables for the process $pp \rightarrow t (\rightarrow b\ell^+\nu_\ell) \bar{t} (\rightarrow \bar{b}\ell^-\bar{\nu}_\ell) H$ that are linearly dependent on the scalar (κ_t) and pseudoscalar ($\tilde{\kappa}_t$) top-Higgs coupling and hence sensitive to the corresponding relative sign. The proposed observables are based on triple product (TP) structures that we extract from the expression of the differential cross section in terms of the spin vectors of the top and antitop quarks. In order to explore other possibilities, we progressively modify these TPs, first by combining them, and then by replacing the spin vectors by the lepton momenta or the t and \bar{t} momenta by their visible parts. Assuming an integrated luminosity that is consistent with that envisioned for the HL-LHC, we find that the most promising observable can disentangle the hypotheses $\kappa_t = 1, \tilde{\kappa}_t = \pm 1$ by more than the $\sim 20\sigma$ statistical level (**N: OK to keep “disentangle” here or do we need to change to something like “can disentangle the hypotheses with effective separations of order...?”**). In the case of observables that do not need the reconstruction of the t and \bar{t} momenta, the power of discrimination is up to the $\sim 16\sigma$ statistical level for the same number of events. We also show that the capability of the most promising observables for separating the CP-mixed hypotheses prevails even when a number of events plausible within the short term LHC is considered.

* mileo@fisica.unlp.edu.ar

† knkiers@taylor.edu

‡ szynkman@fisica.unlp.edu.ar

§ dkcrane@mtu.edu

¶ ethan_gegner@taylor.edu

I. INTRODUCTION

After the discovery of a new boson H by the ATLAS [1] and CMS [2] collaborations, it has become of crucial importance to determine its physical properties with the highest possible precision. The study of the new boson's couplings to fermions is of great relevance and will allow us to better understand this particle's CP-transformation properties, as well as the extent to which this particle is consistent with the Higgs boson predicted by the Standard Model (SM) of particle physics. It is of particular importance to test the coupling of the putative Higgs boson to the top quark. This coupling governs the main Higgs boson production mechanism (which proceeds via gluon fusion) and it contributes to the important Higgs boson decay mode to two photons. It is also involved in the scalar-field naturalness problem – giving rise to the leading dependence on the cut-off energy scale in the corrections to the Higgs mass – and it may play an important role in the mechanism for electroweak symmetry breaking.

Given that the main Higgs boson production process is dominated by a top quark loop and that the diphoton and digluon decay channels are also mediated by a top loop, these processes provide constraints on the scalar and pseudoscalar tH couplings, κ_t and $\tilde{\kappa}_t$ [3–6]. However, these constraints assume that there are no other sources contributing to the corresponding effective couplings; furthermore, in the case of the diphoton decay channel (which also involves a W boson loop), it is also assumed that the coupling of the Higgs boson to the W is standard. In this sense, the constraints derived from measurements of Higgs boson production and decay rates are indirect constraints. Electric dipole moments can also impose stringent indirect constraints on $\tilde{\kappa}_t$ by assuming that there are no new physics (NP) particles contributing to the loops of the relevant diagrams and in the case of the EDM of the electron that the electron-Higgs coupling is that predicted by the SM [3, 7]. In order to probe the tH coupling directly, processes with smaller cross sections need to be taken into account.

In contrast to the τH coupling, which can be studied through the decay $H \rightarrow \tau^+ \tau^-$ [8], the tH coupling can only be tested directly via production processes, since the Higgs boson is kinematically forbidden from decaying to a $t\bar{t}$ pair. Two types of processes are of particular interest in this regard – the production of a Higgs boson in association with a $t\bar{t}$ pair and in association with a single top or antitop. The cross section for associated Higgs production with a single top (antitop) is smaller than that for production with a $t\bar{t}$ pair, and involves the interference between a diagram in which the Higgs is radiated from the top (antitop) leg and one with the Higgs emitted from the intermediate virtual W boson. Interestingly, this implies that the constraints on κ_t and $\tilde{\kappa}_t$ derived from tH and $\bar{t}H$ production are dependent on the assumption made regarding the coupling of the Higgs boson to the W gauge boson, κ_W . Nevertheless, it is important to note that the interference between the above mentioned diagrams can be exploited to determine the relative sign between κ_t and κ_W (see for example Ref. [9]). Associated Higgs production with a $t\bar{t}$ pair has been studied by several authors, and various observables sensitive to the couplings κ_t and $\tilde{\kappa}_t$ have been proposed. Examples of such observables (all of which are CP-even) are the cross section, invariant mass distributions, the transverse Higgs momentum distribution and the azimuthal angular separation between the t and \bar{t} , to name a few [10]. Also, an approach based on weighted moments and optimal observables has been developed in Ref. [11] to discriminate the hypothesis of a CP-even Higgs from that of a CP-mixed state within the context of an e^+e^- as well as a pp collider. Now, CP-even observables are not sensitive to the relative sign between the scalar and pseudoscalar couplings κ_t and $\tilde{\kappa}_t$. Such observables are quadratically dependent on these couplings and thus only provide an indirect measure of CP violation. In order to be sensitive to the relative sign

between κ_t and $\tilde{\kappa}_t$, CP-odd observables must be considered.

Since the top quark decays before it can hadronize, its spin information is passed on to the angular distributions of its decay products in such a way that these particles work as spin analyzers. As is well known, in the case of semileptonic top decay, the charged lepton is the most powerful in this regard. It is also known that the top quark and antiquark spins are highly correlated in $t\bar{t}$ production, a feature that is manifested in the double angular distributions of the decay products of the t and \bar{t} systems [12]. In the case of $t\bar{t}H$ associated production, the $t\bar{t}$ spin correlations are also sensitive to the manner in which the top couples to the Higgs boson. In fact, observables that exploit the differences in the $t\bar{t}$ spin configurations were used in Ref. [13] to improve the discrimination of the $t\bar{t}H$ signal from the dominant irreducible background $t\bar{t}b\bar{b}$, which does not involve the Higgs boson.

In this paper, we define a set of observables that are linearly dependent on κ_t and $\tilde{\kappa}_t$ and are thus sensitive to the relative sign of these couplings. The proposed observables are based on a particular set of triple product (TP) structures that we extract naturally from the expression for the differential cross section for $pp \rightarrow t (\rightarrow b\ell^+\nu_\ell) \bar{t} (\rightarrow \bar{b}\ell^-\bar{\nu}_\ell) H$, making use of the fact that the t and \bar{t} decay products contain spin information and are sensitive to the nature of the tH coupling, as noted above. By using spinor techniques we relate the top and antitop spin vectors to final state particle momenta and separate the production process from the decay. This allows to identify straightforwardly the contributions linearly sensitive to the couplings. Further, the TPs correlations in these contributions incorporate the t and \bar{t} spin vectors. Starting with these TPs, we not only recover the observables given in [10, 14] but also propose additional possibilities that increase the sensitivity. In order to establish a hierarchy in the sensitivity of the TPs under analysis we investigate three different types of observables by using simulated events: asymmetries, mean values and angular distributions. We note that TP correlations have been used in [15] in the context of top-quark production and decay and in [16] in the framework of anomalous color dipole operators.

The remainder of this paper is organized as follows. In Sec. II we study the theoretical framework for the process $pp \rightarrow t (\rightarrow b\ell^+\nu_\ell) \bar{t} (\rightarrow \bar{b}\ell^-\bar{\nu}_\ell) H$ and derive a general expression for the differential cross section from which a first set of TP correlations is extracted. In Sec. III we probe the sensitivity of these TPs to the tH coupling by using various CP-odd observables. Subsequent sections are dedicated to explore another possibilities of CP-odd observables. In particular, observables based on TPs that incorporate the Higgs momentum are discussed in Sec. IV, whereas observables obtained without using the t and \bar{t} momenta are studied in Sec. V. Finally, Sec. VI is devoted to the discussion on the experimental feasibility of the most promising observables encountered here. The main conclusions are summarized in Sec. VII.

II. THEORETICAL FRAMEWORK FOR $pp \rightarrow t(\rightarrow b\ell^+\nu_\ell)\bar{t}(\rightarrow \bar{b}\ell^-\bar{\nu}_\ell)H$

At the LHC $t\bar{t}H$ production proceeds via $q\bar{q}$ annihilation and gg fusion processes. The relevant leading-order Feynman diagrams are displayed in Fig. 1, where the first two rows show the $q\bar{q}$ and gg s -channel diagrams, and the last one depicts the gg t -channel diagrams. Three more gg -initiated diagrams are obtained by exchanging the gluon lines in the third row. We describe the tH coupling with the effective Lagrangian

$$\mathcal{L}_{t\bar{t}H} = -\frac{m_t}{v}(\kappa_t\bar{t}t + i\tilde{\kappa}_t\bar{t}\gamma_5 t)H, \quad (1)$$

where $v = 246$ GeV is the SM Higgs vacuum expectation value, and the coefficients κ_t and $\tilde{\kappa}_t$ parameterize the scalar and pseudoscalar interaction, respectively. The SM case is obtained for $\kappa_t = 1$ and $\tilde{\kappa}_t = 0$, while the values $\kappa_t = 0$ and $\tilde{\kappa}_t \neq 0$ parameterize a CP-odd Higgs boson.

Before turning to a discussion of CP-odd observables, it is useful to consider a few theoretical aspects of the process $pp \rightarrow t(\rightarrow b\ell^+\nu_\ell)\bar{t}(\rightarrow \bar{b}\ell^-\bar{\nu}_\ell)H$, in which the top and antitop both decay semileptonically. In the following subsections we derive a “factorized” expression for the gluon fusion contribution to this process and then use this expression to isolate various mathematical quantities that will be useful as we construct CP-odd observables.

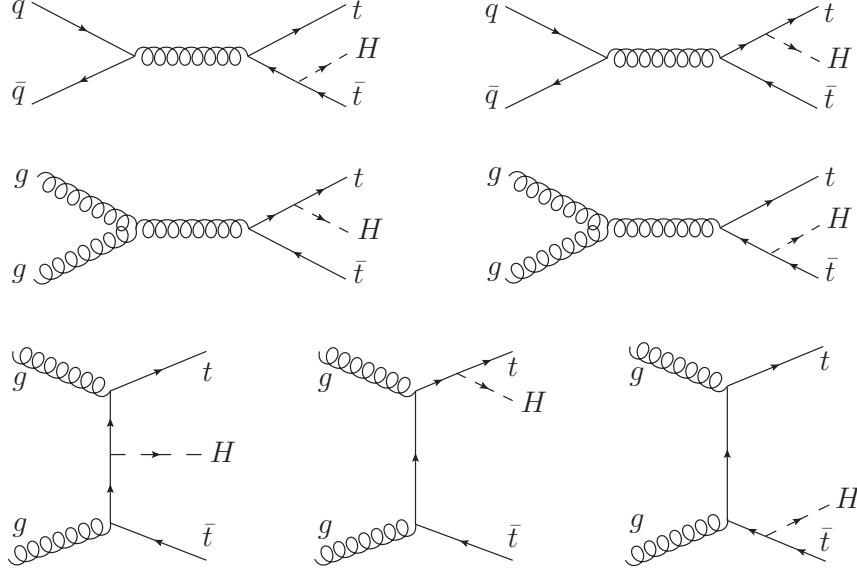


FIG. 1: Tree-level Feynman diagrams contributing to $t\bar{t}H$ production at the LHC. Three more diagrams are obtained by exchanging the gluon lines in the t -channel diagrams.

A. Factorized expression for the scattering cross section

In this subsection we focus on the gg -initiated contributions to $t\bar{t}H$ production, since these dominate over the the quark-antiquark annihilation contributions. As we shall show below, assuming the narrow width approximation for the top and antitop quarks, the unpolarized differential cross section for $gg \rightarrow t(\rightarrow b\ell^+\nu_\ell)\bar{t}(\rightarrow \bar{b}\ell^-\bar{\nu}_\ell)H$ may be written in the following “factorized” form,¹

$$d\sigma = \sum_{\substack{b\ell^+\nu_\ell \\ \text{spins}}} \sum_{\substack{\bar{b}\ell^-\bar{\nu}_\ell \\ \text{spins}}} \left(\frac{2}{\Gamma_t} \right)^2 d\sigma(gg \rightarrow t(n_t)\bar{t}(n_{\bar{t}})H) d\Gamma(t \rightarrow b\ell^+\nu_\ell) d\Gamma(\bar{t} \rightarrow \bar{b}\ell^-\bar{\nu}_\ell), \quad (2)$$

¹ The reader is referred to the discussion following Eq. (17) for some qualifying remarks regarding the “factorization” of this expression.

where $d\sigma(gg \rightarrow t(n_t)\bar{t}(n_{\bar{t}})H)$ is the differential cross section for the production of a top and antitop quark, with spin vectors n_t and $n_{\bar{t}}$, respectively, along with a Higgs boson. Also, $d\Gamma(t \rightarrow b\ell^+\nu_\ell)$ and $d\Gamma(\bar{t} \rightarrow \bar{b}\ell^-\bar{\nu}_\ell)$ are the partial differential decay widths for an unpolarized top and anti-top quark. The four-vectors n_t and $n_{\bar{t}}$ are not arbitrary, but are given by particular combinations of the momenta of the t, \bar{t}, ℓ^+ and ℓ^- [17],

$$n_t = -\frac{p_t}{m_t} + \frac{m_t}{(p_t \cdot p_{\ell^+})}p_{\ell^+} \quad (3)$$

$$n_{\bar{t}} = \frac{p_{\bar{t}}}{m_t} - \frac{m_t}{(p_{\bar{t}} \cdot p_{\ell^-})}p_{\ell^-}. \quad (4)$$

Expressions similar to Eq. (2) have been derived previously for the production of short-lived particles in e^-e^+ colliders [18] and for $t\bar{t}$ production both in e^-e^+ colliders [17] and pp colliders [19].



FIG. 2: Schematic representation of the process $g_a g_b \rightarrow t(\rightarrow b_i \ell^+ \nu_\ell) \bar{t}(\rightarrow \bar{b}_j \ell^- \bar{\nu}_\ell) H$. The indices i, j denote the colour of the quarks while a, b are gluon indices.

To derive the above expressions, we begin by considering the schematic representation for the process $g_a g_b \rightarrow t(\rightarrow b_i \ell^+ \nu_\ell) \bar{t}(\rightarrow \bar{b}_j \ell^- \bar{\nu}_\ell) H$ that is sketched in Fig. 2. Here a and b denote the initial-state gluons and i and j refer to the colours of the top and antitop quarks. The amplitude for this process may be written in the following compact form

$$\mathcal{M}^{ab,ij} = \bar{\psi}_t \mathcal{A}^{ab,ij} \psi_{\bar{t}}, \quad (5)$$

where the spinors $\bar{\psi}_t$ and $\psi_{\bar{t}}$ contain all of the information regarding the decay of the virtual top and anti-top, respectively, and where the quantity $\mathcal{A}^{ab,ij}$ is given by

$$\mathcal{A}^{ab,ij} \equiv A_{\mu\nu}^{ab,ij}(\epsilon_{\lambda_a})^\mu(\epsilon_{\lambda_b})^\nu = \sum_{k=1}^8 \mathcal{A}_k^{ab,ij} = \kappa_t \sum_{k=1}^8 \mathcal{S}_k^{ab,ij} + i\tilde{\kappa}_t \sum_{k=1}^8 \mathcal{P}_k^{ab,ij}. \quad (6)$$

The sum over k in the above expression corresponds to the eight gluon-initiated diagrams indicated in Fig. 1; also, ϵ_{λ_a} and ϵ_{λ_b} are the polarization vectors corresponding to g_a and g_b , respectively. In the last equality in Eq. (6) we have explicitly separated the amplitude into two sums, with one sum corresponding to the scalar contributions and the other to the pseudoscalar

ones. Taking all of the final-state particles to be massless, we can use the spinor techniques developed in [20] to write $\bar{\psi}_t$ and $\psi_{\bar{t}}$ as follows²

$$\bar{\psi}_t = -g^2 \mathbb{P}_t(t) \mathbb{P}_W(t-b) \langle b - |\nu_\ell + \rangle \langle \ell^+ + | (\not{t} + m_t) \quad (7)$$

$$\psi_{\bar{t}} = g^2 \mathbb{P}_t(\bar{t}) \mathbb{P}_W(\bar{t} - \bar{b}) \langle \bar{\nu}_\ell + | \bar{b} - \rangle (\not{\bar{t}} - m_t) |\ell^- + \rangle, \quad (8)$$

where $|i + (-)\rangle \equiv (1/2)(1 \pm \gamma^5) \psi_i$ represents a right-handed (left-handed) chiral spinor for final-state particle i and $\langle i + (-)|$ represents the corresponding adjoint spinor. Also, $\mathbb{P}_t(q) = (q^2 - m_t^2 + im_t \Gamma_t)^{-1}$ and $\mathbb{P}_W(q) = (q^2 - m_W^2 + im_W \Gamma_W)^{-1}$, and we have denoted the momenta of the various particles by the symbols that refer to the names of those particles [21].

Using the expressions defined above for $\bar{\psi}_t$ and $\psi_{\bar{t}}$, we can write the amplitude $\mathcal{M}^{ab,ij}$ in a form that is (in a sense) factorized. As a first step, we insert Eqs. (7) and (8) into Eq. (5), yielding

$$\mathcal{M}^{ab,ij} = -g^4 \mathbb{P}_t(t) \mathbb{P}_t(\bar{t}) \mathbb{P}_W(t-b) \mathbb{P}_W(\bar{t}-\bar{b}) \langle b - |\nu_\ell + \rangle \langle \bar{\nu}_\ell + | \bar{b} - \rangle \sqrt{2(t \cdot \ell^+)} \sqrt{2(\bar{t} \cdot \ell^-)} [\bar{\phi}_t \mathcal{A}^{ab,ij} \phi_{\bar{t}}], \quad (9)$$

where the spinors ϕ_t and $\phi_{\bar{t}}$ are defined as

$$\phi_t = \frac{(\not{t} + m_t)}{\sqrt{2(t \cdot \ell^+)}} |\ell^+ + \rangle \quad (10)$$

$$\phi_{\bar{t}} = \frac{(\not{\bar{t}} - m_t)}{\sqrt{2(\bar{t} \cdot \ell^-)}} |\ell^- + \rangle. \quad (11)$$

Note that in writing down the above expressions we have adopted the narrow-width approximation for the top and antitop quarks and for the W^\pm gauge bosons.³ Working out the projection operators $\phi_t \bar{\phi}_t$ and $\phi_{\bar{t}} \bar{\phi}_{\bar{t}}$, we have

$$\phi_t \bar{\phi}_t = \frac{1}{2} (1 + \not{t} \gamma^5) (\not{t} + m_t) \quad (12)$$

and

$$\phi_{\bar{t}} \bar{\phi}_{\bar{t}} = \frac{1}{2} (1 + \not{\bar{t}} \gamma^5) (\not{\bar{t}} - m_t), \quad (13)$$

with n_t and $n_{\bar{t}}$ being the four-vectors defined in Eqs. (3) and (4). Thus, ϕ_t and $\phi_{\bar{t}}$ may be regarded as describing a top quark with spin vector n_t and an antitop quark with spin vector $n_{\bar{t}}$, respectively.

As a final step toward factorizing the amplitude $\mathcal{M}^{ab,ij}$, we note that the amplitude for a top quark with spin vector n_t to decay into $b\ell^+\nu_\ell$ is given by

$$\mathcal{M}(t(n_t) \rightarrow b\ell^+\nu_\ell) = ig^2 \mathbb{P}_W(t-b) \langle b - |\nu_\ell + \rangle \sqrt{2(t \cdot \ell^+)}, \quad (14)$$

² These spinor techniques can also be used for massive final-state particles. Given the energy scale involved in the process in question, however, the assumption of massless final-state particles is sensible and greatly simplifies the derivation of Eq. (2).

³ Since Eq. (9) contains the top quark propagator term $\mathbb{P}_t(t)$, for example, $|\mathcal{M}^{ab,ij}|^2$ contains the factor $((t^2 - m_t^2)^2 + m_t^2 \Gamma_t^2)^{-1}$, which is replaced by $(\pi/m_t \Gamma_t) \delta(t^2 - m_t^2)$ in the narrow-width approximation. Thus, except for the propagator terms $\mathbb{P}_t(t)$ and $\mathbb{P}_t(\bar{t})$, we take the four-vector t appearing in Eqs. (9)-(11) to be on shell, satisfying $t^2 = m_t^2$.

and likewise,

$$\mathcal{M}(\bar{t}(n_{\bar{t}}) \rightarrow \bar{b}\ell^-\bar{\nu}_\ell) = ig^2\mathbb{P}_W(\bar{t} - \bar{b})\langle\bar{\nu}_\ell + |\bar{b}-\rangle\sqrt{2(\bar{t}\cdot\ell^-)}.\quad (15)$$

Furthermore, the term inside the square brackets in Eq. (9) is the amplitude for producing a top quark with spin vector n_t , along with an anti-top with spin vector $n_{\bar{t}}$ and a Higgs boson,

$$\mathcal{M}(g_ag_b \rightarrow t^i(n_t)\bar{t}^j(n_{\bar{t}})H) = \bar{\phi}_t\mathcal{A}^{ab,ij}\phi_{\bar{t}}.\quad (16)$$

Combining Eqs. (14)-(16), we can write Eq. (9) in a form that appears to be factorized,

$$\mathcal{M}^{ab,ij} = \mathbb{P}_t(t)\mathbb{P}_{\bar{t}}(\bar{t})\mathcal{M}(t(n_t) \rightarrow b\ell^+\nu_\ell)\mathcal{M}(\bar{t}(n_{\bar{t}}) \rightarrow \bar{b}\ell^-\bar{\nu}_\ell)\mathcal{M}(g_ag_b \rightarrow t^i(n_t)\bar{t}^j(n_{\bar{t}})H). \quad (17)$$

It is important to note that, even though the above expression has the appearance of being factorized into production and decay parts, this apparent factorization is a bit misleading. In particular, the amplitude for $t\bar{t}H$ production contains the top and antitop quark spin four-vectors n_t and $n_{\bar{t}}$, which depend on final-state kinematical quantities [see Eqs. (3) and (4)]. With this qualification in mind, we may now use the amplitude in Eq. (17) to determine the corresponding scattering cross section. After some manipulation of the phase space variables to take advantage of the presence of the propagator terms, $\mathbb{P}_t(t)$ and $\mathbb{P}_{\bar{t}}(\bar{t})$, we arrive at the expression in Eq. (2).⁴ This expression also has the appearance of being factorized, but qualifying remarks, similar to those above, apply.

B. Origin of triple product terms

The expression derived above for the scattering cross section [see Eq. (2), as well as Eq. (17)] provides significant insight into how one might analyze $pp \rightarrow t(\rightarrow b\ell^+\nu_\ell)\bar{t}(\rightarrow \bar{b}\ell^-\bar{\nu}_\ell)H$ in order to determine the nature of the top-Higgs coupling. In particular, let us focus on the production amplitude, $\mathcal{M}(g_ag_b \rightarrow t^i(n_t)\bar{t}^j(n_{\bar{t}})H)$, which forms part of the overall amplitude in Eq. (17). The absolute value squared of the production amplitude is used to determine $d\sigma(gg \rightarrow t(n_t)\bar{t}(n_{\bar{t}})H)$, which in turn forms part of the expression for the “factorized” cross section in Eq. (2). Summing over colour and gluon indices we have

$$\sum_{\substack{a,b \\ i,j}} |\mathcal{M}(g_ag_b \rightarrow t^i(n_t)\bar{t}^j(n_{\bar{t}})H)|^2 = \sum_{\substack{a,b \\ i,j}} \left| \sum_{k=1}^8 C_k^{ab,ij} \bar{\phi}_t(\kappa_t\mathcal{S}_k + i\tilde{\kappa}_t\mathcal{P}_k)\phi_{\bar{t}} \right|^2, \quad (18)$$

where we have separated the colour structure of each diagram by defining $\mathcal{S}_k^{ab,ij} = C_k^{ab,ij}\mathcal{S}_k$ and $\mathcal{P}_k^{ab,ij} = C_k^{ab,ij}\mathcal{P}_k$ [see Eqs. (6) and (16)]. Also, the factors $g_s^2m_t/v$ and $-ig_s^2m_t/v$ arising from the vertices of the t - and s -channel diagrams respectively have been included in the definition of $C_k^{ab,ij}$ for convenience. The terms linear in κ_t and $\tilde{\kappa}_t$ can be written as

$$\mathcal{O}(\kappa_t\tilde{\kappa}_t) \rightarrow \frac{1}{2}\kappa_t\tilde{\kappa}_t \sum_{k,r} \mathbb{C}_{kr} \text{Im} \left\{ \text{Tr} \left[(1 + \not{n}_t\gamma^5)(\not{\ell} + m_t)\mathcal{S}_k(1 + \not{n}_{\bar{t}}\gamma^5)(\not{\bar{\ell}} - m_{\bar{t}})\tilde{\mathcal{P}}_r \right] \right\}, \quad (19)$$

⁴ The reader may note that in the differential widths of $t \rightarrow b\ell^+\nu_\ell$ and $\bar{t} \rightarrow \bar{b}\ell^-\bar{\nu}_\ell$ appearing in Eq. (2), the spin states of the top and antitop have been averaged. Interestingly, under the assumption of massless final-state particles, the amplitudes $\mathcal{M}(t(-n_t) \rightarrow b\ell^+\nu_\ell)$ and $\mathcal{M}(\bar{t}(-n_{\bar{t}}) \rightarrow \bar{b}\ell^-\bar{\nu}_\ell)$ vanish.

where the factor $\mathbb{C}_{kr} = \sum_{ab,ij} C_k^{ab,ij} C_r^{ab,ij*}$ is real and where $\tilde{\mathcal{P}}_r = \gamma^0 \mathcal{P}_r^\dagger \gamma^0$. The only terms that yield non-zero contributions in the above sum are those with an odd number of γ^5 matrices; these lead to triple-product (TP) structures of the form $\epsilon_{\alpha\beta\gamma\delta} p_a^\alpha p_b^\beta p_c^\gamma p_d^\delta$, where p_a - p_d represent various four momenta associated with the process. In contrast, it can be seen from Eq. (18) that the terms proportional to κ_t^2 and $\tilde{\kappa}_t^2$ descend from traces containing an even number of γ^5 matrices and can be written in terms of scalar products of the available momenta.

With the above considerations in mind, it is useful to write a general expression for the differential cross section $d\sigma(gg \rightarrow t(n_t)\bar{t}(n_{\bar{t}})H)$ in terms of the momenta $q = (q_1 - q_2)/2$, $Q = (q_1 + q_2)/2$, t , \bar{t} , n_t and $n_{\bar{t}}$, where $q_{1,2}$ denote the momenta of the initial-state gluons. Note that with this choice, $q \cdot Q = 0$ and $Q^2 = -q^2 = M_{t\bar{t}H}^2/4$, where $M_{t\bar{t}H}$ is the invariant mass of the $t\bar{t}H$ system. Fifteen TPs can be constructed from these six four-vectors,⁵ so that

$$d\sigma(gg \rightarrow t(n_t)\bar{t}(n_{\bar{t}})H) = \kappa_t^2 f_1(p_i \cdot p_j) + \tilde{\kappa}_t^2 f_2(p_i \cdot p_j) + \kappa_t \tilde{\kappa}_t \sum_{l=1}^{15} g_l(p_i \cdot p_j) \epsilon_l, \quad (20)$$

where $\epsilon_l = \epsilon_{\alpha\beta\gamma\delta} p_a^\alpha p_b^\beta p_c^\gamma p_d^\delta$ denotes the l th TP (we adopt the convention $\epsilon_{0123} = +1$) and where p_i and p_j refer to any of the six momenta. The functions $f_{1,2}$ and g_k depend only on the possible scalar products and are therefore even under a parity transformation (P). However, the terms linear in $\kappa_t \tilde{\kappa}_t$ are P-odd due to the presence of the P-odd TPs. Hence, only the functions $f_{1,2}$ will contribute to the total cross-section, whereas the TP terms will be sensitive to the sign of the anomalous coupling $\tilde{\kappa}_t$. Of the fifteen TPs mentioned above, we will focus on those that contain both of the spin vectors n_t and $n_{\bar{t}}$, but do not include q . The decision not to consider q -dependent TPs is motivated by the fact that q cannot be expressed in terms of the momenta of final state particles (as Q can, by virtue of energy-momentum conservation). The decision to focus on TPs that contain both n_t and $n_{\bar{t}}$ is rooted in the fact that the spins of pair-produced top and antitop quarks are highly correlated at hadron colliders (even though the quarks themselves are unpolarized). Observables that combine the decay products of the t and \bar{t} will be sensitive to this spin correlation [23]. A similar behaviour is expected in $t\bar{t}H$ production, where it can be shown that single-spin asymmetries vanish [13, 14]. Hence, in order to construct observables sensitive to the structure of the tH coupling, we will restrict our attention to those TPs that include information on the decay products of both the top and anti-top quarks. Only five of the fifteen TPs in Eq. (20) do not involve the four vector q and, among these, only three include both n_t and $n_{\bar{t}}$. Thus, we will restrict our attention to the following TPs

$$\epsilon_1 \equiv \epsilon(t, \bar{t}, n_t, n_{\bar{t}}), \quad (21)$$

$$\epsilon_2 \equiv \epsilon(Q, \bar{t}, n_t, n_{\bar{t}}), \quad (22)$$

$$\epsilon_3 \equiv \epsilon(Q, t, n_t, n_{\bar{t}}). \quad (23)$$

Before turning to a consideration of various CP-odd observables, we remark that even though all of the above discussion took place within the context of gg -initiated production, similar conclusions are obtained for $q\bar{q}$ -initiated production. In particular, the definitions of the spin vectors in Eqs. (3)-(4) and the general form of $d\sigma$ introduced in Eq. (20) are valid in both cases.

⁵ We note that these fifteen TPs are not linearly independent (see the epsilon relations discussed in Ref. [22]).

III. CP-ODD OBSERVABLES

In this section we present three types of observables based on the TPs discussed in Sec. II, namely, asymmetries, angular distributions and mean values. These observables are sensitive not only to the magnitude of the pseudoscalar coupling $\tilde{\kappa}_t$, but also to its sign. In order to test the various observables, we have used `MadGraph5_aMC@NLO` [24] to simulate the process $pp \rightarrow t (\rightarrow b\ell^+\nu_\ell) \bar{t} (\rightarrow \bar{b}\ell^-\bar{\nu}_\ell) H$ at parton level for different values of the couplings κ_t and $\tilde{\kappa}_t$. In all cases we have generated 10^5 events and have assumed a center-of-mass energy of 14 TeV.⁶ We have also imposed the following set of cuts: p_T of leptons > 10 GeV, $|\eta|$ of leptons < 2.5 , $|\eta|$ of b jets < 2.5 and $\Delta R_{\ell\ell} > 0.4$. Note that we have used this somewhat large number of events (10^5) in order to determine clearly the extent to which the proposed observables are sensitive to the NP coupling. Section VI contains an analysis of the experimental feasibility of the more promising observables.

Before continuing on to our analysis, let us make a few comments regarding the values that we choose for κ_t and $\tilde{\kappa}_t$. First of all, we note that if the pseudoscalar coupling $\tilde{\kappa}_t$ is the only source of physics beyond the SM, then indirect constraints (based on the signal strength of $gg \rightarrow H \rightarrow \gamma\gamma$) disfavour $\kappa_t < 0$ but do not resolve the degeneracy in the sign of $\tilde{\kappa}_t$ [10]. On the other hand, if one assumes that the tensor structure of the Higgs interactions are the same as those of the SM and if one parameterizes these interactions via one universal Higgs coupling to vector bosons, κ_V , and one universal Higgs coupling to fermions, κ_f , then the measured signal strengths provided by the ATLAS and CMS collaborations are compatible with the values predicted by the SM, (namely, $\kappa_f = 1$ and $\kappa_V = 1$). With these facts in mind, we will, for the most part, set the value of the scalar coupling to its SM value ($\kappa_t = 1$) and will allow the pseudoscalar coupling to take on various values (including both possible signs). In particular, we analyze the cases $\tilde{\kappa}_t = 0, \pm 0.25, \pm 0.5, \pm 0.75, \pm 1$. In addition, we also provide some analysis regarding the pure CP-odd case ($\kappa_t = 0, \tilde{\kappa}_t = 1$).

A. Asymmetry

The first type of CP-odd observable that we will consider is an asymmetry that compares the number of events for which a given TP is positive to that for which it is negative. Normalizing to the total number of events, we define

$$\mathcal{A}(\epsilon) = \frac{N(\epsilon > 0) - N(\epsilon < 0)}{N(\epsilon > 0) + N(\epsilon < 0)}. \quad (24)$$

By construction, $\mathcal{A} \in [-1, +1]$. Based on the general expression given in Eq. (20), we expect the following functional form for the asymmetry,

$$\mathcal{A}(\epsilon) = \frac{A\kappa_t\tilde{\kappa}_t}{B\kappa_t^2 + C\tilde{\kappa}_t^2}, \quad (25)$$

which for $\kappa_t = 1$ can be parameterized as

$$\mathcal{A}(\epsilon) = \frac{a\tilde{\kappa}_t}{1 + b\tilde{\kappa}_t^2}, \quad (26)$$

⁶ Note that, since we generate the same number of events in each case, the corresponding integrated luminosities are different, since the cross section depends on the value of $\tilde{\kappa}_t$.

where the parameter $a \equiv A/B$ determines the sensitivity to the pseudoscalar coupling, whereas $b \equiv C/B$ quantifies the deviation from linear behaviour.

Table I shows numerical results for the asymmetries associated with three different TPs, ϵ_1 , ϵ_2 and ϵ_3 , taking $\kappa_t = 1$ and $\tilde{\kappa}_t = 0, \pm 1$. The asymmetry \mathcal{A} is shown in each case, along with $\mathcal{A}/\sigma_{\mathcal{A}}$, where $\sigma_{\mathcal{A}}$ is the corresponding statistical uncertainty. As is evident from the table, the asymmetries in question provide a clear separation between the SM and the CP-mixed cases, with typical deviations being of order 10σ . Furthermore, the asymmetries for the SM case are each statistically consistent with zero, as one would expect. The three asymmetries also allow one to determine the sign of $\tilde{\kappa}_t$, with the $\tilde{\kappa}_t = \pm 1$ cases effectively separated by more than 20σ . The sensitivity of the asymmetry is quite similar for the three TPs, as can be seen by including other values of $\tilde{\kappa}_t$ and using the expression in Eq. (26) as a fitting function (see Fig. 3). Performing such a fit, we obtain $(a = -0.057 \pm 0.006, b = 0.5 \pm 0.2)$, $(a = -0.056 \pm 0.006, b = 0.5 \pm 0.2)$ and $(a = 0.058 \pm 0.006, b = 0.6 \pm 0.2)$ for ϵ_1 , ϵ_2 and ϵ_3 , respectively.

The results shown in Table I and Fig. 3 all assume a pp initial state, which is actually a combination of events coming from gg and $q\bar{q}$ initial states. While this combination of initial states is the appropriate scenario to consider, it is interesting to consider the relative contributions to the asymmetry coming from the gg and $q\bar{q}$ initial states. Figure 4 shows three curves for the “ ϵ_1 ” case, one for gg -initiated events, one for $q\bar{q}$ -initiated events, and one for the usual combination of these events (the “ pp ” initial state). Interestingly, we see from Fig. 4 that the asymmetry for this TP is enhanced for gg -initiated production, while it is reduced and of opposite sign for the $q\bar{q}$ -initiated events. The asymmetry for the pp case is evidently dominated by the gg contribution, but is somewhat smaller in magnitude due to the $q\bar{q}$ contribution.

TABLE I: Asymmetries for three different scenarios, obtained by using 10^5 simulated events for the TPs $\epsilon_1 = \epsilon(t, \bar{t}, n_t, n_{\bar{t}})$, $\epsilon_2 = \epsilon(Q, \bar{t}, n_t, n_{\bar{t}})$ and $\epsilon_3 = \epsilon(Q, t, n_t, n_{\bar{t}})$. The three scenarios correspond to the SM ($\kappa_t = 1$ and $\tilde{\kappa}_t = \pm 0$) and two CP-mixed cases (defined by $\kappa_t = 1$ and $\tilde{\kappa}_t = \pm 1$).

κ_t	$\tilde{\kappa}_t$	$\mathcal{A}(\epsilon_1)$	$\mathcal{A}(\epsilon_1)/\sigma_{\mathcal{A}}$	$\mathcal{A}(\epsilon_2)$	$\mathcal{A}(\epsilon_2)/\sigma_{\mathcal{A}}$	$\mathcal{A}(\epsilon_3)$	$\mathcal{A}(\epsilon_3)/\sigma_{\mathcal{A}}$
1	-1	0.0315	10.0	0.0332	10.5	-0.0307	-9.7
1	0	-0.0021	-0.7	0.0009	0.3	-0.0011	-0.3
1	1	-0.0379	-12.0	-0.0411	-13.0	0.0378	12.0

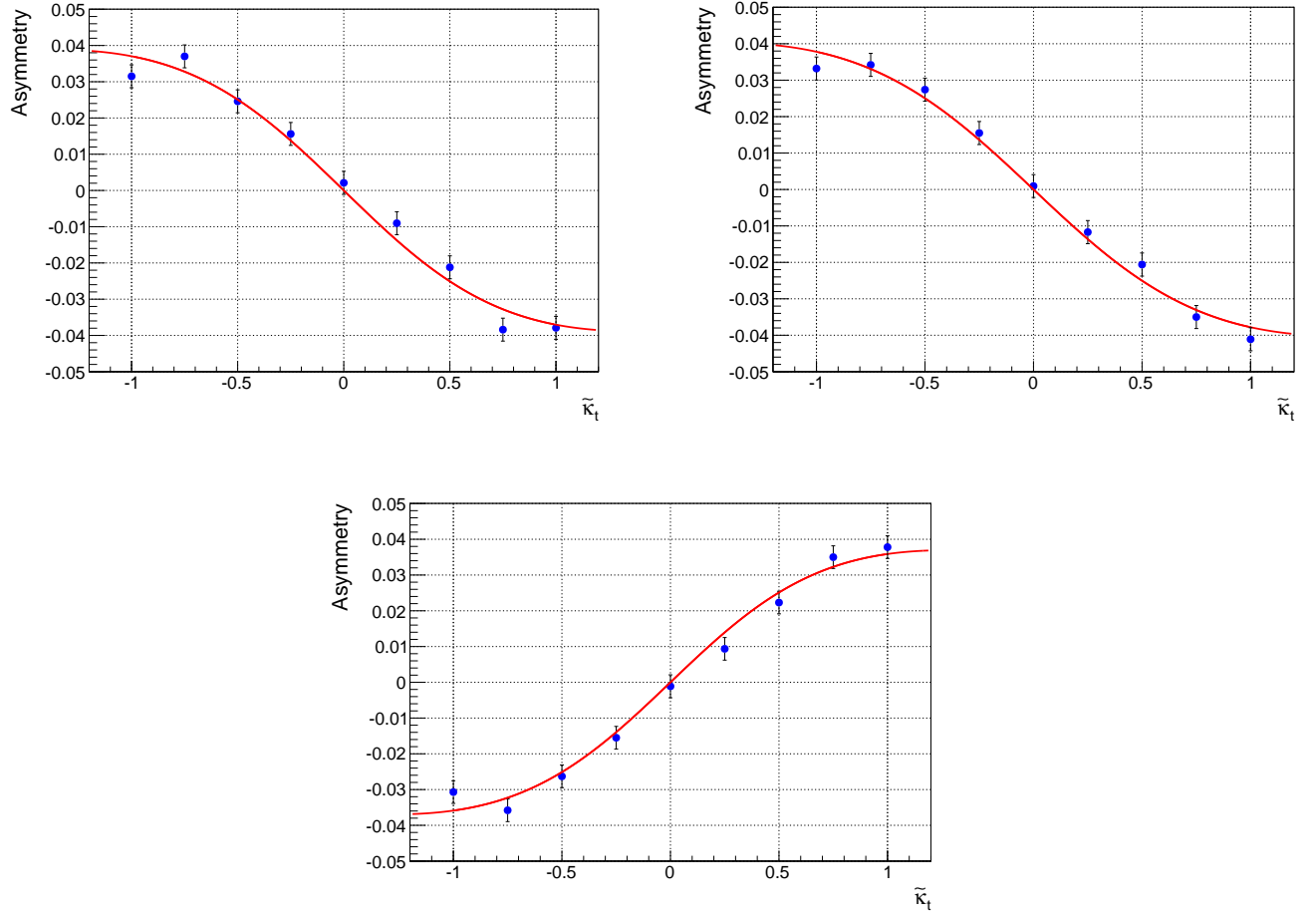


FIG. 3: Asymmetries for the TPs $\epsilon_1 = \epsilon(t, \bar{t}, n_t, n_{\bar{t}})$ (top-left), $\epsilon_2 = \epsilon(Q, \bar{t}, n_t, n_{\bar{t}})$ (top-right) and $\epsilon_3 = \epsilon(Q, t, n_t, n_{\bar{t}})$ (bottom). The points represent the values for $\tilde{\kappa}_t = 0, \pm 0.25, \pm 0.5, \pm 0.75, \pm 1$ and the red solid line is the fitting curve.

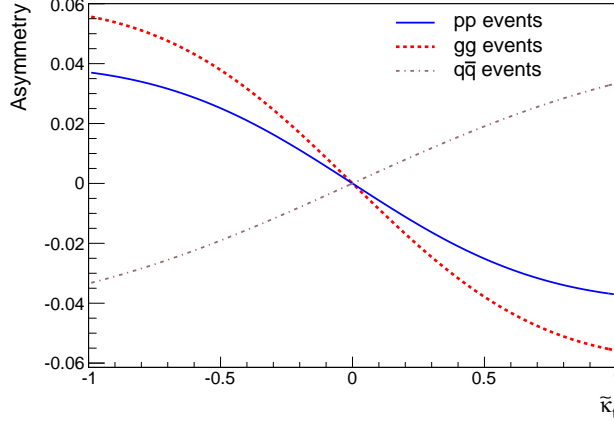


FIG. 4: Asymmetry for the TP $\epsilon_1 = \epsilon(t, \bar{t}, n_t, n_{\bar{t}})$. The dashed line (red) corresponds to gg -initiated production, the dot-dashed line (grey) to $q\bar{q}$ -initiated production and the solid line (blue) to pp production.

We have also tested various linear combinations of the TPs $\epsilon_{1,2,3}$ and have found that the asymmetry is enhanced for the following combination:

$$\epsilon_4 = \epsilon_3 - \epsilon_2 = \epsilon(Q, t - \bar{t}, n_t, n_{\bar{t}}). \quad (27)$$

Note that in the Q rest frame, $\epsilon_4 = Q^0(\vec{t} - \vec{\bar{t}}) \cdot (\vec{n}_t \times \vec{n}_{\bar{t}})$ and the sign of this TP is determined by the quantity $(\vec{t} - \vec{\bar{t}}) \cdot (\vec{n}_t \times \vec{n}_{\bar{t}})$. **(KK: try to connect previous sentences to something later on. . . .)** The values obtained for the asymmetry associated with this TP are shown in Table II. By comparing the results in Tables I and II, we see that the capability of this asymmetry to distinguish **(N: Do we add “effectively” ?)** between the two CP-mixed hypotheses is increased by at least 3σ .

TABLE II: Asymmetry for the TP ϵ_4 for the SM case and the two CP-mixed cases defined by $\kappa_t = 1, \tilde{\kappa}_t = \pm 1$. The values are obtained by using 10^5 simulated events.

κ_t	$\tilde{\kappa}_t$	$\mathcal{A}(\epsilon_4)$	$\mathcal{A}(\epsilon_4)/\sigma_{\mathcal{A}}$
1	-1	-0.0371	-12
1	0	0.0004	0.1
1	1	0.0461	14

Finally, it is worth noting that the asymmetries described in this subsection are not useful for discriminating between the SM hypothesis ($\kappa_t = 1, \tilde{\kappa}_t = 0$) and the pure pseudoscalar hypothesis ($\kappa_t = 0, \tilde{\kappa}_t = 1$). Since the numerators of the asymmetries are all linear in both κ_t and $\tilde{\kappa}_t$, they

are expected to vanish in these cases. However, we will show in the next subsection that there exist angular distributions derived from the TPs that are actually suitable for distinguishing between these two hypotheses.

B. Angular Distributions

Given a certain TP, it is possible to define associated angular distributions that are sensitive to the pseudoscalar coupling $\tilde{\kappa}_t$. In order to clarify this, let us first consider the TP $\epsilon(t, \bar{t}, n_t, n_{\bar{t}})$. This TP can be written as $\epsilon(t + \bar{t}, \bar{t}, n_t, n_{\bar{t}})$, so that in the reference frame defined by $\vec{t} + \vec{\bar{t}} = 0$ and $\vec{t} \parallel \hat{z}$ we have

$$\epsilon(t + \bar{t}, \bar{t}, n_t, n_{\bar{t}}) = M_{t\bar{t}} |\vec{t}| (\vec{n}_t \times \vec{n}_{\bar{t}})_z = M_{t\bar{t}} |\vec{t}| |\vec{n}_t| |\vec{n}_{\bar{t}}| \sin \theta_{n_t} \sin \theta_{n_{\bar{t}}} \sin \Delta\phi(n_t, n_{\bar{t}}), \quad (28)$$

where $M_{t\bar{t}}$ is the invariant mass of the $t\bar{t}$ pair, the angles θ_{n_t} and $\theta_{n_{\bar{t}}}$ denote the polar angles of \vec{n}_t and $\vec{n}_{\bar{t}}$, respectively, and $\Delta\phi(n_t, n_{\bar{t}})$ is the angular difference between the projections of \vec{n}_t and $\vec{n}_{\bar{t}}$ onto the plane perpendicular to \vec{t} . If we define the angle $\Delta\phi(n_t, n_{\bar{t}})$ to be within the range $[-\pi, \pi]$, we see from Eq. (28) that its sign will determine the sign of the TP. Thus, the distribution of the number of events with respect to the angle $\Delta\phi(n_t, n_{\bar{t}})$ is related to the asymmetry of the TP,

$$\mathcal{A}(\epsilon) = 1 - 2 \frac{N(\epsilon < 0)}{N_T} \quad \text{and} \quad \frac{N(\epsilon < 0)}{N_T} = \int_{-\pi}^0 \frac{1}{N_T} \frac{dN}{d\Delta\phi(n_t, n_{\bar{t}})} d\Delta\phi(n_t, n_{\bar{t}}), \quad (29)$$

where N_T is the total number of events. Moreover, for a certain TP one can derive different angular distributions by considering different reference frames, although all of these will satisfy Eq. (29) (note that $\mathcal{A}(\epsilon)$ is Lorentz invariant). Recalling the various TPs considered in Sec. II, we examine the following angular distributions.

1. $\epsilon_1 = \epsilon(t, \bar{t}, n_t, n_{\bar{t}})$. To probe ϵ_1 , we construct the distribution $d\sigma/d\Delta\phi_1(n_t, n_{\bar{t}})$ in the rest frame of $t\bar{t}$, taking \vec{t} to define the z -axis. The angle $\Delta\phi_1(n_t, n_{\bar{t}})$ is the angular difference between the projection of the spin vectors in the plane perpendicular to \vec{t} .
2. $\epsilon_2 = \epsilon(Q, \bar{t}, n_t, n_{\bar{t}})$. In this case, we define the distribution $d\sigma/d\Delta\phi_2(n_t, n_{\bar{t}})$ in the rest frame of Q , taking \vec{t} to define the z -axis. The angle $\Delta\phi_2(n_t, n_{\bar{t}})$ is the angular difference between the projection of the spin vectors in the plane perpendicular to \vec{t} .
3. $\epsilon_3 = \epsilon(Q, t, n_t, n_{\bar{t}})$. The distribution $d\sigma/d\Delta\phi_3(n_t, n_{\bar{t}})$ is also defined in the rest frame of Q , but this time taking \vec{t} to be along the z -axis. The angle $\Delta\phi_3(n_t, n_{\bar{t}})$ is the angular difference between the projection of the spin vectors in the plane perpendicular to \vec{t} .

Figure 5 shows the normalized distributions obtained for the first case listed above. Four scenarios are considered, corresponding to the SM ($\kappa_t = 1$ and $\tilde{\kappa}_t = 0$), two cases in which the Higgs boson has mixed CP couplings ($\kappa_t = 1$ and $\tilde{\kappa}_t = \pm 1$) and a case in which the Higgs boson is purely CP-odd ($\kappa_t = 0, \tilde{\kappa}_t = 1$). Figure 6 shows the analogous distributions for ϵ_2 . The distributions corresponding to ϵ_3 are similar to those of ϵ_2 , except that the “shifts” are in the opposite directions for the two mixed-CP cases. Given the similarities of the plots we do not include them here.

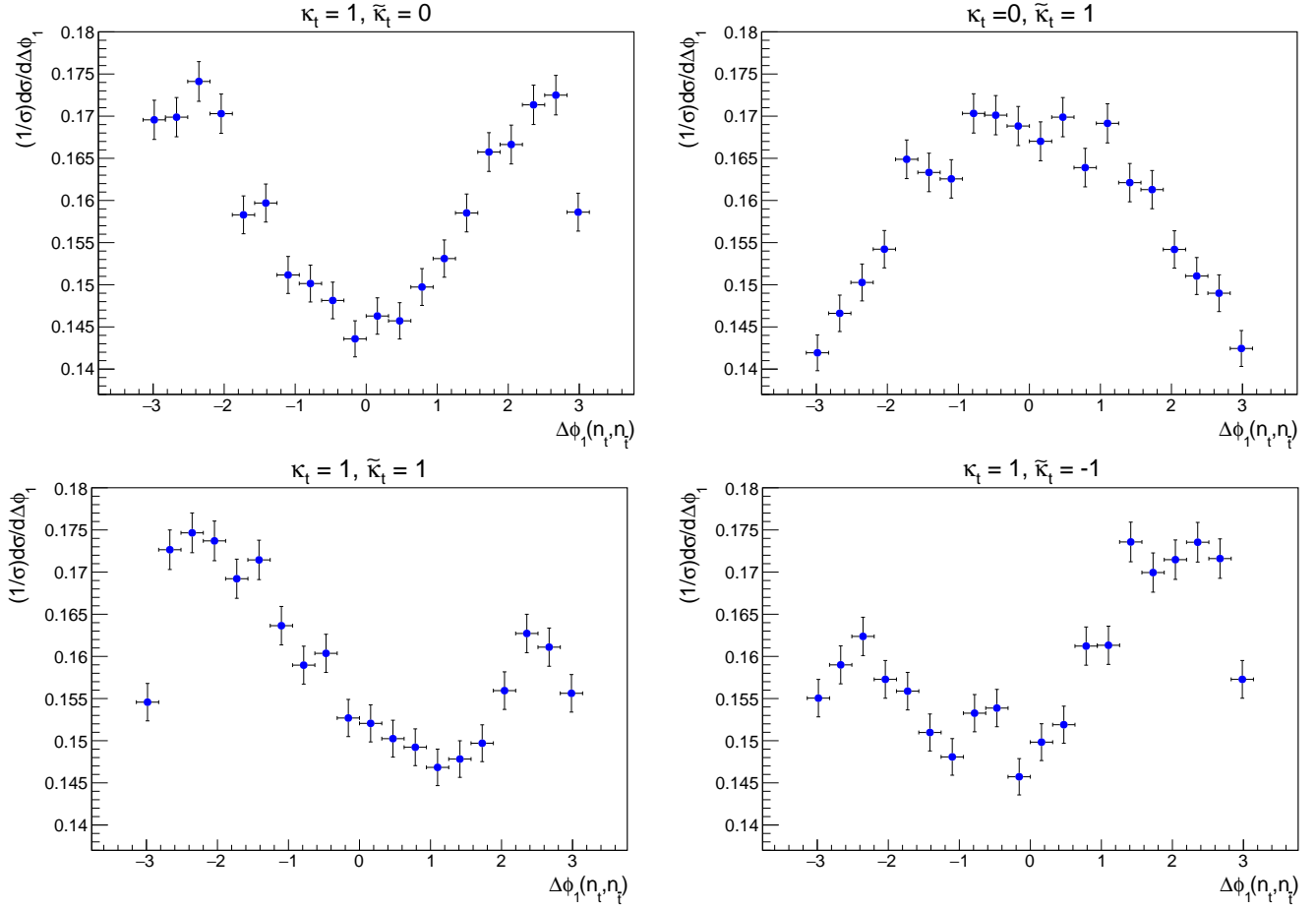


FIG. 5: Angular distributions associated with the TP $\epsilon_1 = \epsilon(t, \bar{t}, n_t, n_{\bar{t}})$ for various values of κ_t and $\tilde{\kappa}_t$. The error bars correspond to the statistical uncertainties.

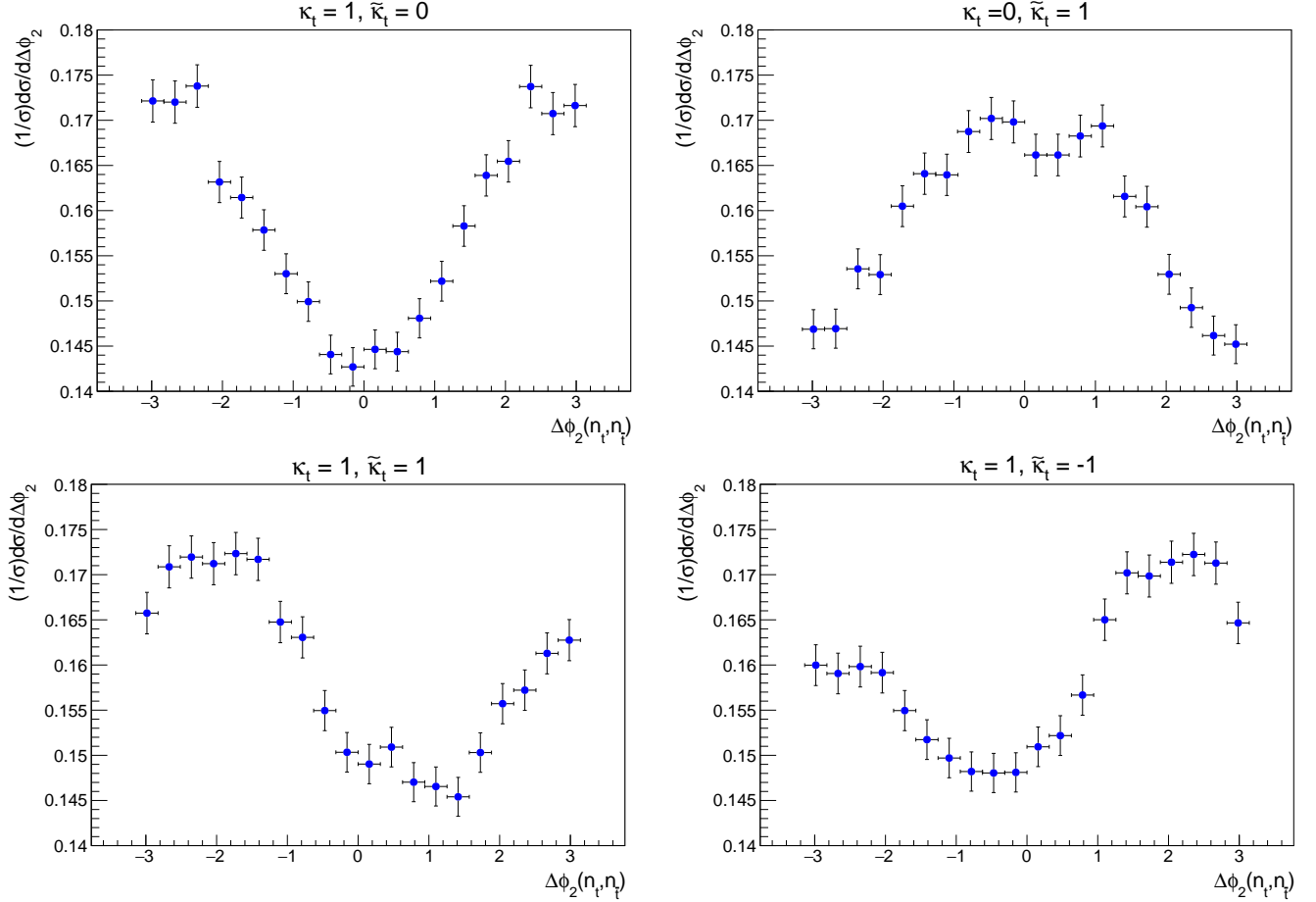


FIG. 6: Angular distributions associated with the TP $\epsilon_2 = \epsilon(Q, \bar{t}, n_t, n_{\bar{t}})$ for various values of κ_t and $\tilde{\kappa}_t$. The error bars indicate the statistical uncertainties.

As can be seen from Figs. 5 and 6, the peaks of the distributions are shifted to the left or the right of the origin in the mixed-CP cases ($\kappa_t = 1$ and $\tilde{\kappa}_t = \pm 1$). The magnitude of the shift appears to be approximately the same in both cases, but is in the opposite direction for $\kappa_t = \tilde{\kappa}_t = 1$ compared to $\kappa_t = -\tilde{\kappa}_t = 1$, thus allowing one to distinguish the sign of the pseudoscalar coupling. The observed dependence on the sign of $\tilde{\kappa}_t$ in these cases is consistent with the fact that the numerator of $\mathcal{A}(\epsilon)$ is linear in $\tilde{\kappa}_t$ [see Eq. (26)] and that the quantity $N(\epsilon < 0)/N_T$ is related to the angular distribution according to Eq. (29). The angular distributions for the SM case ($\kappa_t = 1$ and $\tilde{\kappa}_t = 0$) and the pure pseudoscalar case ($\kappa_t = 0$ and $\tilde{\kappa}_t = 1$) are visibly different from each other and from the mixed-CP scenarios. Comparing the SM and purely pseudoscalar cases, we note that while the angular distributions for the former case exhibit a minimum at $\Delta\phi_{1,2}(n_t, n_{\bar{t}}) = 0$, those for the latter case exhibit a peak at this location. Thus, these two scenarios can be distinguished from each other via these angular distributions. This is to be contrasted with the situation for the asymmetries $\mathcal{A}(\epsilon)$, which vanish in both cases.

In order to quantify the shifts discussed above, we have fitted the simulated distributions with the following function, which was proposed in Ref. [14],

$$\frac{1}{\sigma} \frac{d\sigma}{d\Delta\phi_i(n_t, n_{\bar{t}})} = a_0 + a_1 \cos(\Delta\phi_i(n_t, n_{\bar{t}}) + \delta), \quad i = 1, 2, 3. \quad (30)$$

To the extent that the above expression is exact, we note that Eq. (29) gives $\mathcal{A}(\epsilon_i) = 4a_1 \sin \delta$. With this fitting function, we obtain phase shifts δ that are approximately between 0.9 and 1 (-1 and -0.9) for $\kappa_t = \tilde{\kappa}_t = 1$ ($\kappa_t = -\tilde{\kappa}_t = 1$), both for ϵ_1 and ϵ_2 .⁷ However, the quality of the fits in the four considered scenarios is not very good, particularly for ϵ_1 . The $\chi^2/\text{d.o.f}$ for the fits corresponding to ϵ_1 are in the range 1.69-3.86, while for ϵ_2 they are in the range 0.53-1.16. The deviation from the functional form proposed in Eq. (30) appears to be due primarily to the ΔR_{ll} cut that we have imposed. In fact, when this cut is turned off, the above ranges for the $\chi^2/\text{d.o.f}$ become 0.75-1.14 and 0.44-1.07 for the ϵ_1 and ϵ_2 distributions, respectively. Tables III and IV list the results of the fits obtained when the $\Delta R_{\ell\ell}$ cut is relaxed. Figure 7 shows the corresponding plots for a couple of the scenarios. As is evident from Tables III and IV, the parameter δ is sensitive not only to the modulus of $\tilde{\kappa}_t$ but also to its sign, as would be expected from Eq. (29). The phase shift δ for the $\Delta\phi_1$ distribution appears to exhibit a slightly higher sensitivity than that obtained for the $\Delta\phi_2$ distribution, although the corresponding numerical values obtained for the various scenarios are compatible to within their statistical uncertainties. It is important to stress, however, that the fits for the $\Delta\phi_2$ distributions always yield smaller values for the $\chi^2/\text{d.o.f}$.

TABLE III: Fit results for the angular distribution $d\sigma/(\sigma d\Delta\phi_1(n_t, n_{\bar{t}}))$ (related to the TP $\epsilon_1 = \epsilon(t, \bar{t}, n_t, n_{\bar{t}})$) with the $\Delta R_{\ell\ell}$ cut turned off. Note that the sign of the parameter a_1 changes for $\kappa_t = 0, \kappa_t = 1$, compared to the other cases. We restrict δ to be between $\pm\pi/2$

κ_t	$\tilde{\kappa}_t$	a_0	a_1	δ
1	-1	0.1592 ± 0.0006	-0.0139 ± 0.0008	0.81 ± 0.07
1	0	0.1595 ± 0.0006	-0.0181 ± 0.0008	0.002 ± 0.06
1	1	0.1591 ± 0.0006	-0.0131 ± 0.0008	-0.82 ± 0.07
0	1	0.1591 ± 0.0006	0.0102 ± 0.0008	0.11 ± 0.08

⁷ The results for the TP ϵ_3 are relatively similar to those for ϵ_2 , except that the phase shifts have the opposite sign in the CP-mixed cases. Given this similarity we do not include the corresponding results for the ϵ_3 distribution here.

TABLE IV: Fit results for the angular distribution $d\sigma/(\sigma d\Delta\phi_2(n_t, n_{\bar{t}}))$ (related to the TP $\epsilon_2 = \epsilon(Q, \bar{t}, n_t, n_{\bar{t}})$), with the $\Delta R_{\ell\ell}$ cut turned off. As was the case in Table III, the sign of the parameter a_1 changes for $\kappa_t = 0, \kappa_t = 1$ and we restrict δ to be between $\pm\pi/2$

κ_t	$\tilde{\kappa}_t$	a_0	a_1	δ
1	-1	0.1591 ± 0.0006	-0.0146 ± 0.0008	0.73 ± 0.06
1	0	0.1594 ± 0.0007	-0.0190 ± 0.0008	0.005 ± 0.06
1	1	0.1592 ± 0.0006	-0.0136 ± 0.0008	-0.77 ± 0.07
0	1	0.1591 ± 0.0006	0.0113 ± 0.0008	0.09 ± 0.08

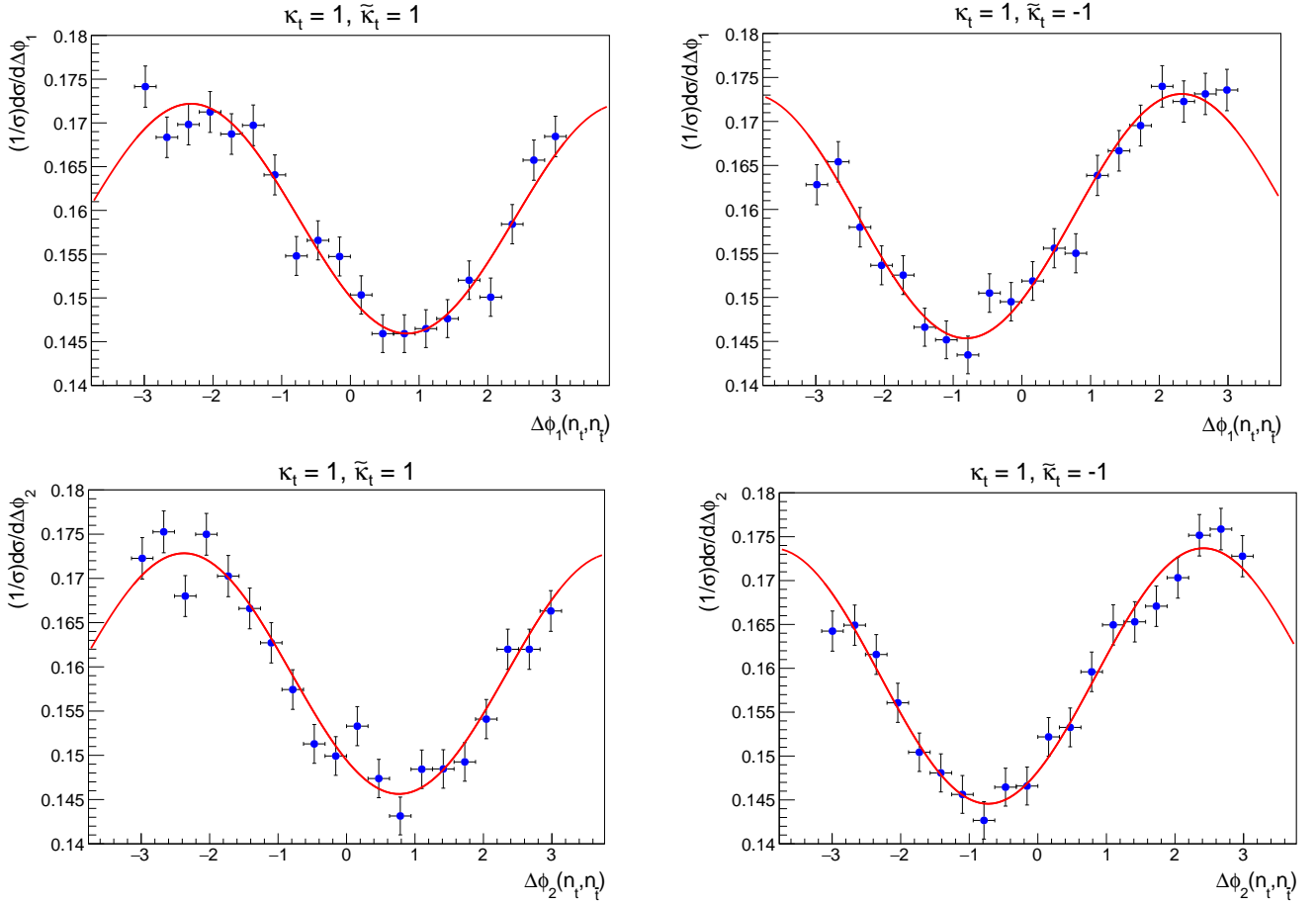


FIG. 7: Angular distributions $d\sigma/(\sigma d\Delta\phi_1(n_t, n_{\bar{t}}))$ (top) and $d\sigma/(\sigma d\Delta\phi_2(n_t, n_{\bar{t}}))$ (bottom) associated with the TPs $\epsilon_1 = \epsilon(t, \bar{t}, n_t, n_{\bar{t}})$ and $\epsilon_2 = \epsilon(Q, \bar{t}, n_t, n_{\bar{t}})$, respectively, for the CP-mixed cases $\kappa_t = \tilde{\kappa}_t = 1$ (left) and $\kappa_t = -\tilde{\kappa}_t = 1$ (right). The $\Delta R_{\ell\ell}$ cut was turned off when generating these results. The corresponding fit curves [see Eq. (30)] are displayed in red.

In Sec. III A we defined a fourth triple product, $\epsilon_4 = \epsilon_3 - \epsilon_2$. We have constructed an angular distribution related to this TP as well. Specifically, we have analyzed the $\Delta\phi(n_t, n_{\bar{t}})$ distribution in the Q rest frame, taking H to define the z -axis. By studying the distributions for various values of κ_t and $\tilde{\kappa}_t$, we have found that they are not well described by Eq. (30) and their range of variation is larger than that of the distributions displayed in Figs. 5 and 6. **(KK: I'm not sure what this means. Are they less cosine-like? Or are the amplitudes or phase shifts larger than those for the other TPs?)** Unlike the distributions related to ϵ_1 - ϵ_3 , those arising from ϵ_4 exhibit small changes in their shapes **(KK: I don't think I understand this, since we said that the range of variation was larger in the last sentence. I think I'm missing something :))** for all the considered hypotheses and for this reason we have not included the corresponding plots here. However, the larger range of variation of the ϵ_4 distributions leads to higher values for the asymmetry (as can be seen from Tables I and II) even when the changes in the respective shapes are smaller **(KK: I don't understand what this means.)** than in the case of the distributions described by Eq. (30).

C. Mean value

We turn now to consider the last type of observable that we will construct from the TPs, the mean value. As was the case for the observables considered in Secs. III A and III B, the mean value is sensitive to $\tilde{\kappa}_t$. Given a certain TP, we define its mean value in the following manner,

$$\langle \epsilon \rangle = \frac{\int \epsilon [d\sigma(pp \rightarrow b \ell^+ \nu_\ell \bar{b} \ell^- \bar{\nu}_\ell H)/d\Phi] d\Phi}{\int [d\sigma(pp \rightarrow b \ell^+ \nu_\ell \bar{b} \ell^- \bar{\nu}_\ell H)/d\Phi] d\Phi}, \quad (31)$$

where Φ is the Lorentz-invariant phase space corresponding to the final state $b \ell^+ \nu_\ell \bar{b} \ell^- \bar{\nu}_\ell H$. From Eq. (20) we see that only the terms linear in (both) κ_t and $\tilde{\kappa}_t$ will contribute to the mean value. Thus, we expect this observable to be sensitive not only to the magnitude of $\kappa_t \tilde{\kappa}_t$, but also to the relative sign of the couplings.

The results obtained for the TPs $\epsilon_1 = \epsilon(t, \bar{t}, n_t, n_{\bar{t}})$, $\epsilon_2 = \epsilon(Q, \bar{t}, n_t, n_{\bar{t}})$ and $\epsilon_3 = \epsilon(Q, t, n_t, n_{\bar{t}})$ introduced in Sec. II are displayed in Table V. For each TP we list the mean value divided by the corresponding statistical uncertainty. We see that the three observables are capable of distinguishing the SM case from both CP-mixed cases. Furthermore, two CP-mixed cases are clearly disentangled, since the the observables are sensitive to the sign of $\tilde{\kappa}_t$. The observables $\langle \epsilon_2 \rangle$ and $\langle \epsilon_3 \rangle$ appear to be slightly more sensitive than $\langle \epsilon_1 \rangle$. On the other hand, the mean value for the combination ϵ_4 introduced in Sec. III A gives slightly smaller values than those listed in Table V, yielding -4.32 , 1.11 and 7.23 for the cases $(\kappa_t = 1, \tilde{\kappa}_t = -1, 0, 1)$, respectively. As with the asymmetry, the purely CP-even and purely CP-odd cases cannot be distinguished by the mean value, since it is linear in both κ_t and $\tilde{\kappa}_t$ (see Eqs. (20) and (31)). Comparing the results in Table V with the results presented in Sec. III A, we can conclude that the sensitivity to the NP contribution is smaller for the mean values of the TPs under consideration than for the corresponding asymmetries.

TABLE V: Mean values obtained for the TPs $\epsilon_{1,2,3}$ for the SM case and two CP-mixed cases. The values are obtained using a sample of 10^5 simulated events.

κ_t	$\tilde{\kappa}_t$	$\langle\epsilon_1\rangle/\sigma_{\tilde{\epsilon}_1}$	$\langle\epsilon_2\rangle/\sigma_{\tilde{\epsilon}_2}$	$\langle\epsilon_3\rangle/\sigma_{\tilde{\epsilon}_3}$
1	-1	4.26	4.94	-5.81
1	0	-0.91	-0.22	1.25
1	1	-7.98	-8.83	8.75

IV. CP-ODD OBSERVABLES NOT DEPENDING ON t AND \bar{t} SPIN VECTORS

So far we have considered three TPs involving the momenta t, \bar{t} and Q and the spin vectors n_t and $n_{\bar{t}}$ [defined in Eqs. (3)-(4)]. Furthermore, we have described the general form of the differential cross-section in terms of these vectors in Eq. (20). In this section we consider other possibilities for the choice of the vectors from which the CP-odd observables can be constructed. From the definitions in Eqs. (3)-(4), we see that the TPs $\epsilon_{1,2,3}$ can be written as follows,

$$\epsilon(t, \bar{t}, n_t, n_{\bar{t}}) = \frac{m_t^2}{(t \cdot \ell^+)(\bar{t} \cdot \ell^-)} \epsilon(t, \bar{t}, \ell^-, \ell^+), \quad (32)$$

$$\epsilon(Q, \bar{t}, n_t, n_{\bar{t}}) = \frac{m_t^2}{(t \cdot \ell^+)(\bar{t} \cdot \ell^-)} \left(\epsilon(t, \bar{t}, \ell^-, \ell^+) + \epsilon(H, \bar{t}, \ell^-, \ell^+) + \frac{(t \cdot \ell^+)}{m_t^2} \epsilon(H, \bar{t}, t, \ell^-) \right), \quad (33)$$

$$\epsilon(Q, t, n_t, n_{\bar{t}}) = \frac{m_t^2}{(t \cdot \ell^+)(\bar{t} \cdot \ell^-)} \left(-\epsilon(t, \bar{t}, \ell^-, \ell^+) + \epsilon(H, t, \ell^-, \ell^+) + \frac{(\bar{t} \cdot \ell^-)}{m_t^2} \epsilon(H, \bar{t}, t, \ell^+) \right). \quad (34)$$

The above equations express the TPs studied in the last sections as linear combination of TPs involving the momenta t, \bar{t}, H, ℓ^+ and ℓ^- , with coefficients that are functions of phase space variables. These five momenta give rise to five TPs whose sensitivity can also be tested by means of the observables introduced in Secs. III A-III C. We have found that TPs that do not include both the lepton and anti-lepton momenta yield negligible sensitivity to the value of $\tilde{\kappa}_t$. For this reason, we concentrate here on the results obtained for the remaining TPs,⁸

$$\epsilon_5 \equiv \epsilon(t, \bar{t}, \ell^-, \ell^+), \quad (35)$$

$$\epsilon_6 \equiv \epsilon(H, t, \ell^-, \ell^+), \quad (36)$$

$$\epsilon_7 \equiv \epsilon(H, \bar{t}, \ell^-, \ell^+). \quad (37)$$

⁸ These TPs should not be confused with those introduced in Eq. (20).

TABLE VI: Asymmetries for the TPs $\epsilon_{5,6,7}$ for the SM case and the two CP-mixed cases defined by $\kappa_t = 1, \tilde{\kappa}_t = \pm 1$. The values correspond to 10^5 simulated events.

κ_t	$\tilde{\kappa}_t$	$\mathcal{A}(\epsilon_5)$	$\mathcal{A}(\epsilon_5)/\sigma_{\mathcal{A}}$	$\mathcal{A}(\epsilon_6)$	$\mathcal{A}(\epsilon_6)/\sigma_{\mathcal{A}}$	$\mathcal{A}(\epsilon_7)$	$\mathcal{A}(\epsilon_7)/\sigma_{\mathcal{A}}$
1	-1	0.0315	10.0	-0.0134	-4.2	0.0111	3.5
1	0	-0.0021	-0.7	-0.0011	-0.3	0.0009	0.3
1	1	-0.0379	-12.0	0.0143	4.5	-0.0137	-4.3

TABLE VII: Mean values obtained for the TPs $\epsilon_{5,6,7}$ for the SM case and two CP-mixed cases with opposite sign in the pseudoscalar coupling. The values correspond to 10^5 simulated events.

κ_t	$\tilde{\kappa}_t$	$\langle\epsilon_5\rangle/\sigma_{\bar{\epsilon}_5}$	$\langle\epsilon_6\rangle/\sigma_{\bar{\epsilon}_6}$	$\langle\epsilon_7\rangle/\sigma_{\bar{\epsilon}_7}$
1	-1	3.98	-1.96	1.69
1	0	-0.43	1.25	0.74
1	1	-6.76	3.46	-3.29

Tables VI and VII summarize the results for the TPs $\epsilon_{5,6,7}$. We see that the TP ϵ_5 gives rise to asymmetries and mean values that are clearly higher than those obtained from ϵ_6 and ϵ_7 . This is in contrast to the TPs $\epsilon_{1,2,3}$, for which the asymmetries and mean values are comparable for the TPs (see Tables I and V). We also note that the asymmetry for ϵ_5 is exactly the same as for ϵ_1 , as is expected from Eq. (32), since the proportionality factor relating them is positive definite. Regarding the mean values, we see by comparing Tables V and VII that the TPs $\epsilon_{1,2,3}$ appear to have a higher sensitivity to the pseudoscalar coupling than $\epsilon_{5,6,7}$.

It is important to mention that in the $t\bar{t}$ rest frame the sign of the TP ϵ_5 is defined through the angle $\Delta\phi_{\ell-\ell^+}$ [see the discussion following Eq. (28)], which is the angular difference between the projections of the leptons' momenta onto the plane perpendicular to \vec{t} . By a similar argument to that discussed at the beginning of Sec. III B, we can construct an associated angular distribution [see Eq. (29)] that will be sensitive to the sign of the pseudoscalar coupling. This angular variable is the same as that proposed in Ref. [14] as a useful CP-odd observable. Moreover, it is shown in Ref. [14] that the corresponding angular distribution follows the functional form given in Eq. (30). The associated shifts (δ) obtained for different values of $\tilde{\kappa}_t$ are expected to be of the same order as those exhibited by the $\Delta\phi_1(n_t, n_{\bar{t}})$ distribution since this distribution is constrained by the asymmetry $\mathcal{A}(\epsilon_5)$ [via Eq. (29)], which in turn is equal to $\mathcal{A}(\epsilon_1)$. Also, we note that $\mathcal{A}(\epsilon_5)$ is slightly smaller than $\mathcal{A}(\epsilon_2)$, as can be seen from Table I.

In analogy with the combination of TPs considered in Sec. III, we have found a combination

of the TPs $\epsilon_{5,6,7}$ for which the asymmetry is enhanced with respect to ϵ_5 - ϵ_7 ,

$$\epsilon_8 = 2\epsilon_5 - \epsilon_6 + \epsilon_7 = \epsilon(t + \bar{t} + H, t - \bar{t}, \ell^+, \ell^-). \quad (38)$$

We see from Eq. (38) that in the $t\bar{t}H$ rest frame $\epsilon_8 = M_{t\bar{t}H}(\vec{t} - \vec{\bar{t}}) \cdot (\vec{\ell}^+ \times \vec{\ell}^-)$, where $M_{t\bar{t}H}$ is the invariant mass of the $t\bar{t}H$ system. Hence, in the $t\bar{t}H$ rest frame the sign of ϵ_8 is determined by the quantity $(\vec{t} - \vec{\bar{t}}) \cdot (\vec{\ell}^+ \times \vec{\ell}^-)$. Comparing Eqs. (27) and (38) and noting that $Q = (t + \bar{t} + H)/2$, we see that the only relevant difference between ϵ_4 and ϵ_8 is that in the latter the spin vectors n_t and $n_{\bar{t}}$ have been replaced by the momenta of the leptons ℓ^+ and ℓ^- , respectively. The values obtained for $\mathcal{A}(\epsilon_8)$ are shown in Table VIII. Compared to the TPs ϵ_1 - ϵ_3 and ϵ_5 - ϵ_7 (see Tables I and VI), the asymmetry for ϵ_8 has a comparable or slightly higher sensitivity for resolving the CP-mixed cases. Comparing with $\mathcal{A}(\epsilon_4)$, however, we see that using the momenta of the leptons (in ϵ_8) instead of the spin vectors produces a decrease in the sensitivity of the asymmetry (see Tables II and VIII).

Having defined the TPs ϵ_5 - ϵ_7 , one can proceed, as in Sec. III B, to define corresponding angular distributions. Of course, in this case the corresponding angles will be defined in terms of the momenta of the leptons instead of using the spin vectors. The angular distributions based on ϵ_5 - ϵ_7 have the same overall behaviour as those derived from ϵ_1 - ϵ_3 . Using Eq. (30) to fit the distributions and comparing to the results obtained for ϵ_1 - ϵ_3 , we find that the phase shifts (δ) are comparable for the ϵ_5 angular distribution, but are smaller for the ϵ_6 and ϵ_7 distributions.

The mean values of ϵ_8 for the scenarios under consideration are comparable with the values listed in Table VII for ϵ_5 . Concerning the associated angular distributions, their range of variation (**KK: I'm not sure what this means**) is larger than in the case of the distributions related to ϵ_5 - ϵ_7 but exhibit smaller changes in their shapes for the different scenarios and for this reason we do not include here the corresponding plots. (**KK: might need to reword this a bit after clarifying what range of variation means.**)

TABLE VIII: Asymmetry for the TP ϵ_8 for the SM case and the two CP-mixed cases defined by $\kappa_t = 1, \tilde{\kappa}_t = \pm 1$. The values are obtained with 10^5 simulated events.

κ_t	$\tilde{\kappa}_t$	$\mathcal{A}(\epsilon_8)$	$\mathcal{A}(\epsilon_8)/\sigma_{\mathcal{A}}$
1	-1	0.0331	10.5
1	0	0.0023	0.7
1	1	-0.0403	-12.7

V. CP-ODD OBSERVABLES NOT DEPENDING ON t AND \bar{t} MOMENTA

The observables discussed in the preceding sections all involve the momenta of the top and/or anti-top quarks and thus require the full reconstruction of the kinematics of the individual t and \bar{t} systems in order to be measured. Although challenging due to the presence of the two neutrinos in the final state, this can in principle be done by applying a kinematic reconstruction method

such as the neutrino weighting technique [25, 26]. Another possibility is to define observables that do not depend on the t and \bar{t} momenta but instead make use of the momenta of the b and \bar{b} quarks to which the t and \bar{t} decay. In order to construct such observables we will take as our starting point the most sensitive observables studied in Secs. III and IV, namely those associated with the TPs ϵ_4 and ϵ_8 , respectively.

Let us first consider the TP combination ϵ_8 , which is defined in Eq. (38). Replacing the momenta of the t and \bar{t} quarks by the momenta of the b and \bar{b} quarks, respectively, we have a new TP,

$$\epsilon_9 = \epsilon(b + \bar{b} + H, b - \bar{b}, \ell^+, \ell^-). \quad (39)$$

Note that the sign of ϵ_9 is determined by the sign of the quantity $(\vec{b} - \vec{\bar{b}}) \cdot (\vec{\ell}^+ \times \vec{\ell}^-)$ in the $b\bar{b}H$ rest frame. This combination of three vectors (determined in the lab frame instead of the $b\bar{b}H$ rest frame) is used in Ref. [10] to define a CP-odd observable that only depends on lab frame variables. The values of the asymmetry for ϵ_9 are listed in Table IX. Comparing Tables VIII and IX we see that the use of the b and \bar{b} momenta instead of the t and \bar{t} momenta leads to a decrease in the sensitivity of the asymmetry by $\sim 5\sigma$ for $\kappa_t = 1, \tilde{\kappa}_t = \pm 1$. Nevertheless, the observable can still discriminate not only between the two CP-mixed scenarios but also between these and the SM case.

TABLE IX: Asymmetry for the TP ϵ_9 for the SM case and the two CP-mixed cases defined by $\kappa_t = 1, \tilde{\kappa}_t = \pm 1$. The values are obtained with 10^5 simulated events.

κ_t	$\tilde{\kappa}_t$	$\mathcal{A}(\epsilon_9)$	$\mathcal{A}(\epsilon_9)/\sigma_{\mathcal{A}}$
1	-1	0.0171	5.4
1	0	0.0010	0.3
1	1	-0.0247	-7.8

We proceed in a similar manner with the TP ϵ_4 . Starting from Eq. (27) and using the definitions of the spin vectors in Eqs. (3)-(4), we have

$$\epsilon_4 = \frac{m_t^2}{(t \cdot \ell^+) \cdot (\bar{t} \cdot \ell^-)} \epsilon(Q, t - \bar{t}, \ell^-, \ell^+) + \frac{1}{(t \cdot \ell^+)} \epsilon(Q, t, \ell^+, \bar{t}) - \frac{1}{(\bar{t} \cdot \ell^-)} \epsilon(Q, \bar{t}, t, \ell^-). \quad (40)$$

Since the asymmetry is not changed by the presence of an overall positive definite multiplicative factor, let us concentrate instead on the following combination of TPs,

$$\epsilon(Q, t - \bar{t}, \ell^-, \ell^+) + \frac{(\bar{t} \cdot \ell^-)}{m_t^2} \epsilon(Q, t, \ell^+, \bar{t}) - \frac{(t \cdot \ell^+)}{m_t^2} \epsilon(Q, \bar{t}, t, \ell^-). \quad (41)$$

Instead of replacing t and \bar{t} directly by b and \bar{b} , we use the visible contributions, namely $b + \ell^+$ and $\bar{b} + \ell^-$, respectively. This results in the following definition

$$\epsilon_{10} = \epsilon(\tilde{Q}, c_{b\bar{b}}, \ell^-, \ell^+) - w_1 \epsilon(\tilde{Q}, b, \bar{b}, \ell^+) + w_2 \epsilon(\tilde{Q}, b, \bar{b}, \ell^-), \quad (42)$$

where $\tilde{Q} \equiv (b + \ell^+ + \bar{b} + \ell^-)/2$ stands for the visible part of Q , $c_{b\bar{b}} = (1 - w_1)b - (1 - w_2)\bar{b}$, and the weights $w_{1,2}$ are given by $(\bar{b} \cdot \ell^-)/m_t^2$ and $(b \cdot \ell^+)/m_t^2$, respectively. Also, the contribution m_ℓ^2/m_t^2 has been neglected both in w_1 and in w_2 . Note that if we set $w_1 = w_2 = 0$, the combination ϵ_{10} reduces to $\epsilon_9/2$ and $\mathcal{A}(\epsilon_{10})$ becomes equal to $\mathcal{A}(\epsilon_9)$. The results obtained for the asymmetry of ϵ_{10} are given in Table X. By comparing Tables II and X we see again that the sensitivity of the asymmetry decreases when t and \bar{t} are not included in the TP. Nevertheless, the combination ϵ_{10} remains a useful observable for discriminating the CP nature of the Higgs boson, with the corresponding asymmetry having a sensitivity that is higher than that of ϵ_9 .

Comparing Tables IX and X, we see that the separation between the CP-mixed scenarios is enhanced by about 3σ for $\mathcal{A}(\epsilon_{10})$ compared to $\mathcal{A}(\epsilon_9)$. This improvement in the asymmetry may be due to two facts. In the first place, as was pointed out in Sec. IV when comparing the TPs ϵ_4 and ϵ_8 , the asymmetry appears to be higher when the spin vectors are used instead of the lepton momenta. We see from Eqs. (39) and (42) that ϵ_{10} , being obtained from ϵ_4 , contains the information on the spin vectors; by way of contrast, ϵ_9 depends directly on the lepton momenta because it is derived from ϵ_8 . In the second place, in order to obtain ϵ_{10} , we have replaced the top and antitop momenta by their visible parts, while in the case of ϵ_9 the bottom and antibottom momenta have been used.

TABLE X: Asymmetry for the TP ϵ_{10} for the SM case and the two CP-mixed cases defined by $\kappa_t = 1, \tilde{\kappa}_t = \pm 1$. The values are obtained by using 10^5 simulated events.

κ_t	$\tilde{\kappa}_t$	$\mathcal{A}(\epsilon_{10})$	$\mathcal{A}(\epsilon_{10})/\sigma_{\mathcal{A}}$
1	-1	-0.0213	-6.7
1	0	0.0031	1.0
1	1	0.0300	9.5

For comparison purposes, we have also used our simulated events to test the lab frame observable given in Ref. [10]. We have found that this observable appears to be slightly less sensitive than $\mathcal{A}(\epsilon_{10})$, giving rise to a separation between the CP-mixed scenarios that is smaller by about 1.4σ .

VI. EXPERIMENTAL FEASIBILITY

In our numerical analyses so far we have used relatively large samples of events (10^5 events per sample) in order to clearly distinguish which observables would be most promising. The number of events expected at the HL-LHC, however, is smaller than the number of events that we have used in our simulations. In this section we reexamine the more promising observables, using sample sizes that are more attainable in the near future.

Let us first make some estimates regarding the number of signal events expected at the HL-LHC. In Sec. III we introduced several mild selection cuts. Implementing these cuts, and assuming that the final state leptons could be either electrons or muons, the SM cross section for

$pp \rightarrow t (\rightarrow b\ell^+\nu_\ell) \bar{t} (\rightarrow \bar{b}\ell^-\bar{\nu}_\ell) H$ at 14 TeV is $\sim 15.3\text{ fb}$; thus, the number of events expected within the context of the HL-LHC is $\sim 15.3\text{ fb} \times 3000\text{ fb}^{-1} = 4.59 \times 10^4$. This number is expected to be larger if $\tilde{\kappa}_t \neq 0$ (assuming $\kappa_t = 1$), since the corresponding cross section is larger than the SM cross section in this case. Taking into account NLO corrections (to the production process) via a K factor of approximately 1.2 [27–29], we find that the expected number of events increases to $\sim 5.5 \times 10^4$. On the other hand, additional cuts, as well as a reduction in efficiency related to momentum reconstruction, will lead to a decrease in this number. In order to measure the asymmetry $\mathcal{A}(\epsilon_4)$, for example, the t and \bar{t} momenta need to be reconstructed. This is challenging, not only due to the presence of two neutrinos in the final state (which escape the detector undetected), but also because the (visible) quarks and charged leptons in the final state need to be correctly associated with the corresponding parent particle (i.e., the top or antitop quark) [25]. As was already noted in Sec. V, one possibility is to use the neutrino weighting technique along with associated kinematic constraints [25, 26, 30]. Within the context of $t\bar{t}$ production this procedure has been used, for instance, to obtain spin correlation [25] and charge asymmetry [26] measurements. Also, events reconstructed using this technique have been used in the analysis of angular distributions that are useful for discriminating the signal from the backgrounds in $t\bar{t}H(H \rightarrow b\bar{b})$ at the LHC [30]. In all these cases the corresponding efficiencies in the reconstruction of the momenta are of order 80%.

Given the discussion in the previous paragraph, we have generated sets of 5×10^4 , 1×10^4 and 5×10^3 events and have recalculated the most sensitive observable, $\mathcal{A}(\epsilon_4)$, for each case. The results are displayed in Table XI, where it can be seen that for 5×10^4 events (which is close to our rough estimate above for the total number of signal events for the HL-LHC), the observable is still very sensitive to $\tilde{\kappa}_t$. In this case, the CP-mixed scenarios are effectively separated by 19σ . As expected, the sensitivity worsens as the number of events is reduced, but even with 5×10^3 events the effective separation between the CP-mixed scenarios under consideration is $\sim 6.5\sigma$.

In Sec. V we defined the TP combination ϵ_{10} , which does not depend directly on the top or antitop momenta. Although the top and antitop momenta would not need to be reconstructed to measure $\mathcal{A}(\epsilon_{10})$, it is still useful to examine this observable for more conservative numbers of events. Table XII shows the results obtained for 5×10^4 and 1×10^4 events. We see in this case that even with 1×10^4 events the observable is able to distinguish the CP-mixed cases by 5.6σ (**N: Do we add “effectively” distinguish?**).

Finally, it is important to mention that a realistic analysis of the sensitivity of the observables discussed in this paper requires a study of the impact of the backgrounds, as well as the hadronization of the quarks in the final state and the effects of the detector. If we consider the dominant decay mode of the Higgs boson, $H \rightarrow b\bar{b}$, in order to maximize the cross section of the process, the signature is given by 4 b -jets, two leptons and missing energy. The main background arises from the production of $t\bar{t}$ in association with additional jets, with the dominant source being the production of $t\bar{t} + b\bar{b}$. In Ref. [31] it is shown that the application of a small set of cuts results in a large improvement in the signal to background ratio. On the experimental side, a rigorous treatment of the signal and backgrounds for $t\bar{t}H$ production with $H \rightarrow b\bar{b}$ is performed in Ref. [32], using 20.3 fb^{-1} of data at $\sqrt{s} = 8\text{ TeV}$.

The results shown in Tables XI and XII reveal that with 5×10^3 and 1×10^4 events, respectively, the observables $\mathcal{A}(\epsilon_4)$ and $\mathcal{A}(\epsilon_{10})$ are still useful for testing $\tilde{\kappa}_t$. Without taking into account the loss of events that would take place in a realistic experimental analysis, these numbers of events correspond to a luminosity of $\sim 300\text{--}600\text{ fb}^{-1}$ for the SM and even smaller for

TABLE XI: Asymmetry for the TP ϵ_4 obtained using 5×10^4 , 1×10^4 and 5×10^3 events for the SM case and the two CP-mixed cases.

κ_t	$\tilde{\kappa}_t$	$N_{\text{ev}} = 5 \times 10^4$		$N_{\text{ev}} = 1 \times 10^4$		$N_{\text{ev}} = 5 \times 10^3$	
		$\mathcal{A}(\epsilon_4)$	$\mathcal{A}(\epsilon_4)/\sigma_{\mathcal{A}}$	$\mathcal{A}(\epsilon_4)$	$\mathcal{A}(\epsilon_4)/\sigma_{\mathcal{A}}$	$\mathcal{A}(\epsilon_4)$	$\mathcal{A}(\epsilon_4)/\sigma_{\mathcal{A}}$
1	-1	-0.0405	-9.1	-0.0426	-4.3	-0.0496	-3.5
1	0	0.0004	0.1	-0.0084	-0.8	-0.0004	-0.03
1	1	0.0443	9.9	0.0434	4.2	0.0420	3.0

TABLE XII: Asymmetry for the TP ϵ_{10} in the SM case and the two CP-mixed cases for 5×10^4 and 1×10^4 events.

κ_t	$\tilde{\kappa}_t$	$N_{\text{ev}} = 5 \times 10^4$		$N_{\text{ev}} = 1 \times 10^4$	
		$\mathcal{A}(\epsilon_{10})$	$\mathcal{A}(\epsilon_{10})/\sigma_{\mathcal{A}}$	$\mathcal{A}(\epsilon_{10})$	$\mathcal{A}(\epsilon_{10})/\sigma_{\mathcal{A}}$
1	-1	-0.0270	-6.0	-0.0184	-1.8
1	0	0.0022	0.5	-0.0086	-0.9
1	1	0.0313	7.0	0.0380	3.8

the CP-mixed cases (due to their larger cross section). This range of luminosities is in principle achievable in the short term by the LHC. We note that in order to be fully conclusive about the required luminosity, it is important to include the effects of hadronization, detector resolution, reconstruction efficiencies and so forth. Such an analysis, however, is beyond the scope of this paper.

VII. CONCLUSIONS

In this paper we have presented a collection of CP-odd observables based on triple product correlations in $pp \rightarrow t (\rightarrow b\ell^+\nu_\ell) \bar{t} (\rightarrow \bar{b}\ell^-\bar{\nu}_\ell) H$ that are useful for disentangling the relative sign between the scalar (κ_t) and a potential pseudoscalar ($\tilde{\kappa}_t$) top-Higgs couplings. We have tested the sensitivity of the various triple product correlations by considering three types of observables: asymmetries, angular distributions, and mean values. Using these observables, we have examined several benchmark scenarios, focusing in particular on the SM ($\kappa_t = 1$ and $\tilde{\kappa}_t = 0$) and on two ‘‘CP-mixed’’ scenarios ($\kappa_t = 1$ and $\tilde{\kappa}_t = \pm 1$).

Through the use of spinor techniques we have written the expression for the differential

cross section of the full process in such a manner that the production and the decay parts are separated, although connected by the spin vectors of the top and antitop, which are given in terms of the momenta of the leptons in the final state. Moreover, we have identified the terms linear in κ_t and $\tilde{\kappa}_t$ as those involving TPs. Among these, we have explored the three that do not involve the momenta of the incoming quarks/gluons and at the same time incorporate both spin vectors: $\epsilon_1 \equiv \epsilon(t, \bar{t}, n_t, n_{\bar{t}})$, $\epsilon_2 \equiv \epsilon(Q, \bar{t}, n_t, n_{\bar{t}})$ and $\epsilon_3 \equiv \epsilon(Q, t, n_t, n_{\bar{t}})$.

We have found that $\epsilon_{1,2,3}$ allow one to distinguish between the CP-mixed scenarios by more than $\sim 20\sigma$ in the case of asymmetries and $\sim 10\sigma$ in the case of mean values when 1×10^5 simulated events are used. Furthermore, we have shown that the angular distributions associated with these TPs are also sensitive to the value of κ_t and $\tilde{\kappa}_t$, exhibiting a phase shift that varies according to the values taken by these couplings. By exploring TPs that incorporate the momenta of the Higgs and the leptons instead of the spin vectors, we have concluded that the observables studied here appear to be more sensitive when the spin vectors are used.

We have also proposed a combination of the TPs, $\epsilon_4 \equiv \epsilon_3 - \epsilon_2$, which has a greater sensitivity than ϵ_1 - ϵ_3 . With 1×10^5 events, for example, the asymmetry associated with this TP gives an effective separation between the CP-mixed scenarios that exceeds those coming from ϵ_1 - ϵ_3 by at least 3σ . When a similar combination is constructed by using the leptons' momenta instead of the spin vectors (ϵ_8), the sensitivity in the asymmetry is decreased by $\sim 3\sigma$ compared to the asymmetry associated with ϵ_4 for the same number of events, giving values compatible with those obtained for the asymmetries of ϵ_2 and ϵ_3 .

Taking into account the challenge of reconstructing the top and antitop momenta due to the presence of two neutrinos in the final state, we have proposed and tested two TP correlations that avoid this difficulty. The first one is obtained by replacing the t and \bar{t} momenta by the b and \bar{b} momenta (ϵ_9), whereas the second includes the visible part of the t and \bar{t} momenta (ϵ_{10}). We have found that the latter is the more sensitive of the two, leading to a discrimination of the CP-mixed cases by up to $\sim 16\sigma$.

Finally, we have discussed the experimental feasibility of the most sensitive observables proposed here. We have found that with 5×10^3 and 1×10^4 events, respectively, the asymmetries associated with ϵ_4 and ϵ_{10} are still useful for testing the hypotheses ($\kappa_t = 1, \tilde{\kappa}_t = \pm 1$), giving rise to separations of order $\sim 6\sigma$. These numbers of events are within reach in the short term at the LHC, so that these observables could in principle be used to test the sign of $\tilde{\kappa}_t/\kappa_t$ within that context. **(KK: maybe reword this sentence a bit...?)**

Acknowledgments This work has been partially supported by ANPCyT under grants No. PICT 2013-0433 and No. PICT 2013-2266, and by CONICET (NM, AS). The work of DC, EG and KK was supported by the U.S. National Science Foundation under Grant PHY-1215785.

REFERENCES

- [1] G. Aad *et al.* (ATLAS Collaboration), Physics Letters B **716**, 1 (2012).
- [2] S. Chatrchyan *et al.* (CMS Collaboration), Physics Letters B **716**, 30 (2012).
- [3] J. Brod, U. Haisch, and J. Zupan, Journal of High Energy Physics **2013**, 180 (2013), 10.1007/JHEP11(2013)180.
- [4] J. Ellis and T. You, Journal of High Energy Physics **2013**, 103 (2013), 10.1007/JHEP06(2013)103.

- [5] A. Djouadi and G. Moreau, The European Physical Journal C **73**, 2512 (2013), 10.1140/epjc/s10052-013-2512-9.
- [6] K. Cheung, J. Lee, and P.-Y. Tseng, Journal of High Energy Physics **2013**, 134 (2013), 10.1007/JHEP05(2013)134.
- [7] J. Baron *et al.* (ACME Collaboration), Science **343**, 269 (2014).
- [8] R. Harnik, A. Martin, T. Okui, R. Primulando, and F. Yu, Phys. Rev. D **88**, 076009 (2013).
- [9] M. Farina, C. Grojean, F. Maltoni, E. Salvioni, and A. Thamm, Journal of High Energy Physics **2013**, 22 (2013), 10.1007/JHEP05(2013)022.
- [10] F. Boudjema, D. Guadagnoli, R. M. Godbole, and K. A. Mohan, Phys. Rev. D **92**, 015019 (2015); M. R. Buckley and D. Goncalves, (2015), arXiv:1507.07926 [hep-ph]; G. Li, H.-R. Wang, and S.-h. Zhu, (2015), arXiv:1506.06453 [hep-ph]; Y. Chen, D. Stolarski, and R. Vega-Morales, Phys. Rev. **D92**, 053003 (2015), arXiv:1505.01168 [hep-ph]; S. Khatibi and M. M. Najafabadi, *ibid.* **D90**, 074014 (2014), arXiv:1409.6553 [hep-ph].
- [11] J. F. Gunion and X.-G. He, Phys. Rev. Lett. **76**, 4468 (1996); J. F. Gunion, B. Grzadkowski, and X.-G. He, *ibid.* **77**, 5172 (1996); J. F. Gunion and J. Pliszka, Physics Letters B **444**, 136 (1998); X.-G. He, G.-N. Li, and Y.-J. Zheng, International Journal of Modern Physics A **30**, 1550156 (2015).
- [12] G. Mahlon and S. Parke, Phys. Rev. D **53**, 4886 (1996); Physics Letters B **411**, 173 (1997); Phys. Rev. D **81**, 074024 (2010); D. Atwood, A. Aeppli, and A. Soni, Phys. Rev. Lett. **69**, 2754 (1992).
- [13] S. Biswas, R. Frederix, E. Gabrielli, and B. Mele, Journal of High Energy Physics **2014**, 20 (2014), 10.1007/JHEP07(2014)020.
- [14] J. Ellis, D. Hwang, K. Sakurai, and M. Takeuchi, Journal of High Energy Physics **2014**, 4 (2014), 10.1007/JHEP04(2014)004.
- [15] O. Antipin and G. Valencia, Phys. Rev. D **79**, 013013 (2009); G. Valencia, *Proceedings on 11th International Conference on Heavy Quarks and Leptons (HQL 2012)*, PoS **HQL2012**, 050 (2012), arXiv:1301.0962 [hep-ph].
- [16] A. Hayreter and G. Valencia, Phys. Rev. D **88**, 034033 (2013).
- [17] T. Arens and L. M. Sehgal, Phys. Rev. D **50**, 4372 (1994).
- [18] S. Kawasaki, T. Shirafulji, and S. Y. Tsai, Prog. Theor. Phys. **49**, 1656 (1973).
- [19] P. Saha, K. Kiers, B. Bhattacharya, D. London, A. Szynekman, and J. Melendez, (2015), arXiv:1510.00204 [hep-ph]; P. Saha, K. Kiers, D. London, and A. Szynekman, Phys. Rev. **D90**, 094016 (2014), arXiv:1407.1725 [hep-ph]; K. Kiers, P. Saha, A. Szynekman, D. London, S. Judge, and J. Melendez, **D90**, 094015 (2014), arXiv:1407.1724 [hep-ph]; K. Kiers, T. Knighton, D. London, M. Russell, A. Szynekman, and K. Webster, **D84**, 074018 (2011), arXiv:1107.0754 [hep-ph].

- [20] R. Kleiss and W. Stirling, Nuclear Physics B **262**, 235 (1985).
- [21] M. L. Mangano and S. J. Parke, Physics Reports **200**, 301 (1991).
- [22] H. W. Fearing and S. Scherer, Phys. Rev. D **53**, 315 (1996).
- [23] W. Bernreuther, A. Brandenburg, Z. Si, and P. Uwer, Nuclear Physics B **690**, 81 (2004).
- [24] J. Alwall, R. Frederix, S. Frixione, V. Hirschi, F. Maltoni, O. Mattelaer, H.-S. Shao, T. Stelzer, P. Torrielli, and M. Zaro, Journal of High Energy Physics **2014**, 79 (2014), 10.1007/JHEP07(2014)079.
- [25] *Measurements of spin correlation in top-antitop quark events from proton-proton collisions at $s = 7$ TeV using the ATLAS detector*, Tech. Rep. ATLAS-CONF-2013-101 (CERN, Geneva, 2013).
- [26] G. Aad *et al.* (ATLAS Collaboration), Journal of High Energy Physics **2015**, 61 (2015), 10.1007/JHEP05(2015)061.
- [27] S. Dawson, L. H. Orr, L. Reina, and D. Wackerroth, Phys. Rev. D **67**, 071503 (2003).
- [28] W. Beenakker, S. Dittmaier, M. Kramer, B. Plumper, M. Spira, and P. Zerwas, Nuclear Physics B **653**, 151 (2003).
- [29] S. Dittmaier *et al.* (LHC Higgs Cross Section Working Group), *Handbook of LHC Higgs Cross Sections: 1. Inclusive Observables* (CERN, Geneva, 2011).
- [30] S. P. Amor dos Santos, J. P. Araque, R. Cantrill, N. F. Castro, M. C. N. Fiolhais, R. Frederix, R. Gonalo, R. Martins, R. Santos, J. Silva, A. Onofre, H. Peixoto, and A. Reigoto, Phys. Rev. D **92**, 034021 (2015).
- [31] H.-L. Li, P.-C. Lu, Z.-G. Si, and Y. Wang, (2015), arXiv:1508.06416 [hep-ph].
- [32] G. Aad *et al.* (ATLAS Collaboration), The European Physical Journal C **75**, 349 (2015), 10.1140/epjc/s10052-015-3543-1.